TAMPEREEN TEKNILLINEN YLIOPISTO
TAMPERE UNIVERSITY OF TECHNOLOGY

RASA OZOLINA

SMART DELIVERY SYSTEMS FOR CANCER TREATMENT USING ADVANCED LIPOSOME FORMULATIONS: FABRICATION, SPECTROSCOPIC CHARACTERIZATION AND CELL INTERNALIZATION STUDIES

Master of Science thesis

Supervisors: Dr. Jana B. Nieder,
Dr. Marlene Lúcio
Examiner: Prof. Jari Hyttinen
Examiner and topic approved by the Faculty Council of the Faculty of Computing and Electrical Engineering on 9th December 2015

ABSTRACT

RASA OZOLINA: Smart delivery systems for cancer treatment using advanced liposome formulations: fabrication, spectroscopic characterization and cell internalization studies
Tampere University of technology
Master of Science Thesis, 70 pages, 10 Appendix pages
May 2016
Master's Degree Programme in Electrical Engineering
Major: Biomedical Engineering
Examiner: Professor Jari Hyttinen

Keywords: anticancer liposomal formulation, quenching assay, cell uptake

Cancer is a leading cause of death in the world; consequently, an increasing number of studies have been dedicated to the improvement of cancer therapy treatments over several decades.

The objective of this thesis is to fabricate anti-cancer liposomal formulation, with a novel, improved composition, consisting of lipid vesicles encapsulating anti-cancer drug doxorubicin (DOX) and to spectroscopically characterize these liposomes. In addition, the internalization process of the drug in cells was studied by using advanced fluorescence imaging techniques.

DOX is used for wide variety of cancer types but its main disadvantage is high toxicity for other healthy organs and tissues that can lead to fatal complications. The use of liposomes as carriers of DOX is thus very appealing to counteract this disadvantage and protect the healthy tissues from contact with the DOX toxicity. A number of DOX liposomal formulations using active loading methods have been developed. With these loading methods large amounts of DOX are encapsulated and lead to the formation of dimers, lowering drug activity.

In this work a carrier system made of Dioctadecyldimethylammonium Bromide (DODAB) and 1-oleoyl-*rac*-glycerol (Monoolein (MO)) with a ratio of (1:2) is proposed. This system has recently been described to have the potential of encapsulating drugs, not only at the DODAB enriched bilayer level, but also at the inverted non-lamellar MO-enriched phases at the vesicle interior.

After fabrication the stability of the liposomal system was tested by measuring the size and zeta potential of the liposomes. Four different 'nano-ruler' *n*-(9-anthroyloxy)-stearic acid (*n*-AS) probes at 3^{rd}, 6^{th}, 9^{th} and 12^{th} – carbon positions of an membrane inserted lipid chain were used for determination of the nanoscale localization of DOX inside the liposome bilayer. These studies revealed that DOX is located closest to the 9-AS probe, close to the bilayer center. The internalization of the liposomal formulation in epidermoid and lung carcinoma cells was analyzed using confocal imaging. It was concluded that the formulation with DOX encapsulated in DODAB:MO (1:2) has more controlled drug release compared to the free drug and a commercial formulation, confirming the potential of the developed formulation for cancer treatment.

PREFACE

The words Thomas Jefferson said have proven to be right: “I am a great believer in luck, and I find the harder I work, the more I have of it’’. I have had luck to do my Master studies in Tampere University of Technology and through dedication earned the opportunity to do a collaboration thesis project in INL - International Iberian Nanotechnology Laboratory and University of Minho in Braga, Portugal. Past two years were filled with highs and lows, but above all - growth! I believe I have grown as a person, as a student and as a researcher. This experience has given a great starting point for my career.

I wish to express my gratitude to my supervisors: Dr. Jana B. Nieder for her encouraging guidance, endless ideas and belief in me throughout and beyond the thesis project. Not only did she warmly welcome me in “Ultrafast Bio- and Nanophotonics” group but also shed light over my first steps in research. I sincerely thank Professor Dr. Marlene Lúcio, who kindly instructed whenever I needed help and also taught towards analytical thinking. And last but not least, I thank Professor Jari Hyttinen, who supported the idea of this international and collaborative project from the beginning, for his invaluable advices and for examining my thesis. Special thanks is owed to Vânia Vilas-Boas for her introduction into cell culture techniques and her unique expertise.

I would like to thank all my colleagues from INL and University of Minho for the discussions, friendships and support. Very special thank you to Dr. Edite Figueiras for the crazy idea, the introduction in Portuguese culture, the trips, the laughter and, foremost, the friendship!

Sincere thanks to my friends for their patience, positive attitude and jokes!

Finally, I would like to thank and dedicate this thesis to my family and, especially, to my grandparents. I am grateful for your unconditional love and support. Paldies!

Tampere, 25.5.2016

Rasa Ozoliņa

PUBLICATIONS

Results described in this thesis were partly presented in poster presentations at an international conference, an advanced school on nano-optics and an international meeting on endocytosis trafficking and signalling.

- "*Characterization of Smart Drug Delivery Systems*", Jana B. Nieder, Rasa Ozolina, Ana M. Carvalho, Vânia Vilas-Boas, M.E.C.D. Real Oliveira, Marlene Lúcio; Poster presentation at NanoPT, 16th -19th February 2016, at INL - International Iberian Nanotechnology Laboratory, Braga, Portugal.

- "*Biophysical Characterization, Nanoscale Composition and Cell Uptake Studies of pH-Sensitive Drug Delivery Systems*", Jana B. Nieder, Rasa Ozolina, Ana M. Carvalho, Vânia Vilas-Boas, M.E.C.D. Real Oliveira, Marlene Lúcio; Poster presentation at "14th IUVSTA School on Nano-Optics: from Principles to Basic Research and Applications", April 11th to 15th 2016 at INL - International Iberian Nanotechnology Laboratory, Braga, Portugal.

- "*Application and Development of Advanced Bioimaging Techniques for Nanodrug Cell Delivery Studies*", Rasa Ozolina, Vânia Vilas-Boas, Oscar F. Silvestre, Edite Figueiras, Jana B. Nieder; Poster presentation at SMETS1: 1st Small Meeting on Endocytic Trafficking and Signaling, 28th April to May 3rd 2016, at INL - International Iberian Nanotechnology Laboratory, Braga, Portugal.

RESEARCH INFRASTRUCTURES USED FOR EXPERIMENTS DESCRIBED IN THIS THESIS:

At University of Minho:

- Liposome fabrication facility including extruder system (Northern Lipids Lipex Extruder)
- Dynamic Light Scattering equipment and ELS (Malvern Instruments)

At INL - International Iberian Nanotechnology Laboratory:

- Optical Spectroscopy Facilities:
  - UV-Vis-NIR Spectrometer (Lambda 950, Perkin Elmer)
  - Steady-State Fluorescence Spectrometer (FluoroMax-4, Horiba)
  - Time-Correlated Single Photon Counting based Fluorescence Lifetime Spectrometer (ChronosBH, ISS Inc.) equipped with a 379 nm picosecond diode laser, PT-100 and PMT detector (H7422-40) both from Hamamatsu

- Cell Culture Facility:
  - Equipped besides others with a laminar flow hood (Bio II Advance, Telstar), incubator (CB 150, Binder), bright-field microscope (Nikon Eclipse, TS 100), Neubauer chamber for cell counting

- Advanced Bioimaging Facility:
  - Confocal microscope (LSM 780, Zeiss) equipped with an Argon laser and several solid state lasers providing excitation lines at 405, 488, 514, 532, 561 and 633 nm and with a Zeiss 34 channel Quasar detector, consisting of a regular multi-alkali photomultiplier tube (PMT), a cooled PMT and a 32 channel Gallium-Arsenide-Phosphide (GaAsP) detector. In transmission path a further PMT is mounted. The system is equipped with a top stage incubator system from okolab.

CONTENTS

LIST OF FIGURES

LIST OF SYMBOLS AND ABBREVIATIONS

$[Q]_m$	Effective Concentration in Membrane
A	Acceptor
D	Donor
DLS	Dynamic Light Scattering
DNA	Deoxyribonucleic Acid
DODAB	Dioctadecyldimethylammonium Bromide
DOX	Doxorubicin
DOX@DODAB:MO	DODAB:MO (1:2) liposome with DOX
E	Transfer Efficiency
ELS	Electrophoretic Light Scattering
EPR	Enhanced Permeability and Retention effect
FRET	Fluorescence Resonance Energy Transfer
IRF	Instrument Response Function
K_D	Dynamic Constant
K_p	Partition Coefficient
K_q	Bimolecular Quenching Constants
K_S	Static Constant
K_{SV}	Stern-Volmer Constant
LSCM	Laser Scanning Confocal Microscope
MO	Monoolein (1-oleoyl-*rac*-glycerol)
n-AS	*n*-(9-anthroyloxy)-stearic acid
n-AS@DODAB:MO	DODAB:MO (1:2) liposome containing 3-AS, 6-AS, 9-AS and 12- AS probes
PdI	Polydispersity Index
PSD	Particle Size Distribution
R_0	Förster Distance
RES	Reticuloendothelial System
SDS	Sodium Dodecyl Sulphate
TCSPC	Time Correlated Single Photon Counting
T_m	Gel-to-Liquid Crystalline Phase Transition Temperature
WHO	World Health Organization

1. INTRODUCTION

Despite thorough research over many decades, cancers still figure amongst the leading causes of death. According to the World Health Organization (WHO) in 2012 alone there were 14 million new cases and 8.2 million cancer related deaths worldwide (World Health Organization 2015). 70% increase in new cancer cases is expected by 2030.

Since 1970s doxorubicin (DOX) is used as chemotherapy drug to treat many types of cancer, amongst them are: hematological malignancies (for example, leukaemia and lymphoma), different types of carcinoma (solid tumours) and soft tissue sarcomas (Momparler et al. 1976). The key disadvantage of this anticancer drug is high toxicity to other healthy organs and tissues that can lead to fatal complications.

Novel drug delivery methods using nanocarriers, such as state-of-the-art pH-sensitive liposomes loaded with DOX, show favourable results in counteracting with this disadvantage and protecting the healthy tissues from contact with the DOX toxicity. The first liposomal DOX formulation Doxil® was approved by United States' Food and Drug Administration in 1995 (Barenholz 2012), since then liposomal formulations have been profoundly researched. Marlene Lúcio and Elisabete C.D. Real Oliveira from University of Minho created the Dioctadecyldimethylammonium Bromide (DODAB) and 1-oleoyl-*rac*-glycerol (Monoolein (MO)) - DODAB:MO liposomal formulation, which shows advantageous pH-dependent release and drug-loading characteristics, compared to other liposomal formulations. Full characterization of the phase behaviour and aggregate morphology of DODAB:MO mixtures at different molar ratios have been done (Oliveira et al. 2012). The ratio 1:2 was found to be the most stable and with high encapsulation efficiency (Van Dijck 2013). DODAB:MO has been successfully investigated for small interfering RNA delivery (Oliveira 2016) and potentiality of encapsulating drugs, such as DOX, have been researched (da Rocha 2014).

Currently, there are no studies showing the depth where in the DODAB:MO (1:2) liposome´s lipid bilayer DOX is located. The location of the drug within the bilayer is important in liposome characterization. If the drug is more towards the exterior or the interior of the liposome it could have interesting applications for drug delivery, and, for example, may indicate that it is possible to deliver more drug at once without dimerization occurring. Furthermore, liposome-cell interaction for the specific liposome and cancer cell lines has not been reported.

The aim of this master thesis is to for the first time study DODAB:MO(1:2) liposomal formulation nanoscale location of DOX within the lipid bilayer and investigate liposome-cell interaction. Thus the objective is to spectroscopically characterize pH-dependent liposome formulation and, in addition, internalization process of the DODAB:MO (1:2) loaded with DOX in cells should be analyzed by using advanced fluorescence imaging techniques. This study is the continuation of recently published results of (Silva et al. 2014) who studied effect of incubation temperature on DODAB:MO lipoplex structure.

In order to reach the aim, DODAB:MO (1:2) liposomes were fabricated using thin lipid film hydration method followed by extrusion, and for spectroscopic characterization studies *n*-(9-anthroyloxy)-stearic acid (*n*-AS) probes and varying concentrations of DOX were added. Liposome size and surface charge were determined by dynamic and electrophoretic light scattering, and nanoscale localization of the drug was determined by a fluorescence quenching assay. In addition, using Förster resonance energy transfer (FRET) analysis the distances between DOX and probe molecules were determined. For cellular uptake studies, two different cancer cell lines (A431 and A549) were used. Each cell line was exposed to liposomal formulation with varying DOX concentration, to commercial liposomal formulation Doxil® and free DOX suspension in water solution. Cellular uptake was studied measuring the fluorescence emission signal of DOX using a laser scanning confocal microscope. Fixed cell samples, that were fixed after different time points of exposure to the drug sample solutions, as well as live cells exposed to the DOX-loaded liposomes, and for which time-lapse 3D image series have been recorded, were analysed.

2. SMART DELIVERY SYSTEMS FOR CANCER TREATMENT

Chemotherapy, and especially, anthracyclines, is a powerful strategy that has been widely used for cancer treatment in clinical therapy. Anthracyclines are anti-tumour agents (with antibiotic activity) that interfere with enzymes involved in deoxyribonucleic acid (DNA) replication during all phases of the cell cycle (American Cancer Society 2015). They are used for a wide range of cancers. DOX is a common anthracycline prescribed for cancer treatment. Smart drug delivery systems show several benefits as carriers of anticancer drugs, for example, reduced toxicity of anticancer agents used in chemotherapy and achieve the desired therapeutic effect with lower dose, and, possibly, enhanced efficacy. Liposomes are considered one of the best drug delivery systems for low molecular weight drugs, imaging agents, peptides, proteins, and nucleic acids (Laouini et al. 2012; Lian & Ho 2001).

2.1 Liposomal delivery systems

Liposomes, first discovered in United Kingdom in 1961 by A. D. Bangham, are artificial microscopic spherical-shaped vesicles (Immordino et al. 2006). Research of liposomes expanded over the last years, broadening their application fields from drug and gene delivery to diagnostics, cosmetics, long-lasting immune-contraception to food and chemical industry. Ten liposomal and lipid-based formulations have been approved by regulatory authorities and many liposomal drugs are in preclinical development or in clinical trials (Laouini et al. 2012).

Liposomes have one or multiple concentric lipid bilayers (lamellas) surrounding an internal aqueous compartment. Liposomes´ safety and success as carriers for drugs is in part due to their chemical and structural resemblance with natural cellular membranes. Usually, cell membrane bilayer consists of phospholipids in two monolayers in which the non-polar, hydrocarbon chain groups are facing away from the water and face each other, while the polar, hydrophilic headgroups of the phospholipid are attracted to the water in interior and exterior of the cell (Laouini et al. 2012). This hydrophobic effect is further ensured by intermolecular forces like electrostatic interactions, hydrogen bonding, van der Waals and dispersion forces (Laouini et al. 2012).

Liposome's membrane can be composed of natural and/or synthetic lipids, amino acid surfactants or other materials which have the following properties: biocompatibility, biodegradability and they consist of non-immunogenic material. Liposomes' bilayer

structure is unique and it allows using liposomes as carriers for lipophilic as well as water-soluble molecules. Hydrophilic substances are incorporated in the interior aqueous compartment while lipophilic drugs are mainly trapped within lipid bilayers. Liposome offers protection for both the drug encapsulated and the healthy tissue from the harming mutual influence (Lian & Ho 2001). The attractive biological properties, including the biocompatibility and biodegradability, of liposomes have been affirmed by different authors (Laouini et al. 2012; Lian & Ho 2001). Amongst other advantages are high encapsulation efficiency, and stability against chemical and environmental influences; target-specific delivery of encapsulated drugs, and sustained drug release. Liposome small size (~50-1000 nm) allows relatively higher intracellular uptake than other systems (Laouini et al. 2012).

If liposomes are intravenously administered most of them tend to accumulate in the bone marrow, lymph nodes, spleen, lungs, and liver. Furthermore, solid tumours and sites of inflammation and infection have increased blood flow and vascularisation to feed the cancer cells which tend to divide extremely fast and need nutrition. This leads to increased possibility to accumulate the liposomes close to tumour and inflammation sites - the effect is widely known as enhanced permeability effect (EPR).

Nanoparticles are recognized and removed from the cardiovascular system by the reticuloendothelial system (RES) or the mononuclear phagocyte system before interacting with the cell membrane. pH-sensitive liposomes' size are typically tuned to be smaller than 250 nm and thus less recognized by RES while still big enough to cause the favourable EPR effect. When pH-sensitive liposomes are PEGylated they are able to evade RES and to specifically trigger the release of the loaded drugs in response to the change of pH in the surrounding environment. The liposomes with prolonged circulation time and RES avoidance property were named by Dr. Frank Martin as "stealthy", which means unseen or unrecognized as foreign particulates by the RES.

2.1.1 pH-dependent liposomes

Rapid recognition of conventional liposomes by the cell's RES mainly in liver and spleen leads to short plasma half-lives (time in which liposome loses half of its pharmacologic, physiologic, or radiologic activity) (Elron-Gross et al. 2009). Therefore, their clinical potential is not fully used. Besides, liposomes enter cells mainly via the endocytosis pathway and eventually reach the lysosome within the cell. In the lysosome, liposomes and their encapsulated drugs or genes are exposed to the risk of being degraded by lysosomal enzymes, which will further significantly reduce the drug efficacy (Liu & Huang 2013).

Stimuli-sensitive liposomes are proposed to avoid degradation of loaded drugs in lysosomes and to release their ingredients in one go as a result of destabilization of the

liposome membrane caused by specific stimuli (for example, changes of physiological pH, tissue specific enzymes, temperature or electrolyte concentration, etc.) (Liu & Huang 2013). pH-sensitive liposomes enable the encapsulated drugs to be specifically targeted to cancerous tissues (such as primary tumours, metastases, inflammation etc.) of the body in which pH varies from the normal physiological value. Tumours and inflamed regions are to some extent more acidic with pH of about pH 5.3, when compared to normal tissues with pH 7.4 (Liu & Huang 2013).

pH-sensitive liposomes shall deliver drug or genes into the cell cytoplasm via the endocytosis pathway. Internalization via the endocytosis pathway is stable. Then, liposomes are mainly destabilized in the low pH endosomes and are directly released into the cytoplasm from there being able to reach nucleus or mitochondria targets.

2.1.2 DODAB:MO (1:2) liposomes

The state of the art liposomes investigated in this project are formulations composed of DODAB and MO in a 1:2 ratio.

2.1.2.1 Chemical structure

DODAB is a monovalent cationic surfactant that forms large unilamellar vesicles (LUV's) in excess water. It consists of a double acyl chain (C18:0) bounded to a quaternary ammonium headgroup. This hydrophilic headgroup part gives the single positive charge per molecule, which is screened by the counter-ion bromine (Br^-).

DODAB has a gel-to-liquid crystalline phase transition temperature (T_m) of 45 °C (Silva et al. 2012). Below T_m the lipid is in a solid-crystalline or 'gel' phase, above the T_m it is in a liquid-crystalline or 'fluid' phase. In the liquid-crystalline phase, the lipids are capable to diffuse freely within its plane. In this phase lipids are receptive for drugs to be encapsulated (Berg 1993). DODAB's T_m is high when compared with the human body temperature (37 °C), meaning that DODAB's bilayers are rigid at normal body temperature. Furthermore, DODAB liposomes are highly stable and do not release the drugs instantly when administered.

Other cationic surfactants such as DODAC, where the counter-ion is a chloride (Cl^-), have been researched. However, DODAB forms more densely packed bilayers at the headgroup region than DODAC, and it also exhibits lower T_m values and less toxicity than DODAC.

Although the increased rigidity of DODAB liposomes is an advantage regarding the stability of the liposomes, it may also result in a more difficult encapsulation of the drugs. This limitation can be counteracted by adding a helper lipid with a lower T_m, for example, monoolein (MO), cholesterol and dioleoylphosphatidylethanolamine (DOPE), which will lower the T_m of the lipid formulation (Silva et al. 2012).

MO is a neutral lipid composed by an unsaturated amphiphilic hydrocarbon chain attached to a glycerol backbone by an esther bond. Its amphiphilic molecule nature is due to the hydrophilic headgroup and to the hydrophobic chain. MO degrades by esterase activity in tissue thus MO is biodegradable. Other interesting characteristics of MO are its affordable price, non-toxicity and biocompatibility.

Specific feature of H_2O/MO system is the excess water-phase separation region and formation of two inverted bi-continuous cubic phases. As a result MO forms non-lamellar vesicles with negative curvature. This makes MO an interesting *helper* lipid able to decrease the structural stiffness of DODAB vesicles - lateral mobility of the lipid chain is increased and fusion of the liposomes with the cell membrane is improved. Tuning MO content in DODAB:MO formulations is important for the formulation development for drug delivery purposes. The ratio DODAB:MO (1:2) promotes the formation of lamellar phases of DODAB:MO enclosing a pool of MO inverted non lamellar phases. According to this lipid tuning, these lipid nanocarriers have the advantages of a liposome, containing the same lamellar ordered bilayer that confers stability for the carrier cargo, but do not have an aqueous filled core. Instead, the vesicle core is filled with a sponge-like honeycombed structure rich in MO with internal aqueous channels, where the loading of hydrophilic/lipophilic cargos is very much increased. MO has an additional advantage to lower the net positive charge of the liposome, which decreases transfection-associated cytotoxicity (Silva et al. 2012).

2.1.2.2 State-of-the-art on DODAB:MO(1:2)

Research efforts to improve the safety profile of the DOX by encapsulation into various types of liposomal formulations have shown reduced cardiotoxicity and better survival of the experimental animals compared to the controls receiving free drugs (Laouini et al. 2012). DODAB:MO liposomal systems have been previously investigated for delivery of DNA and bovine serum albumin (Silva et al. 2008; Van Dijck 2013; Oliveira et al. 2015).

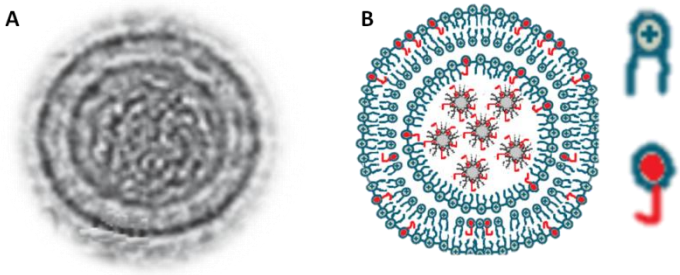

Figure 1. *DODAB:MO (1:2) liposome. A- a cryo-TEM image, B- an adapted schematic model. Adapted from (Oliveira et al. 2012)*

In this study, the DODAB:MO (2:1) liposomal formulation for the first time is studied in the frame of a nano drug carrier for the well known anti-cancer drug DOX in terms of

nanoscale drug localization and cell uptake characterization. The liposomal formulation was chosen because of its potential to increase the DOX loading efficiency without risking dimerization of the drug. The DODAB:MO liposomes have single lipid bilayer structure, but MO can be found also in non-lamellar structures inside the core of the liposome (Figure 1). The bilayer is mostly composed of DODAB, but with some MO lipids randomly dispersed throughout. As MO has a bent shape and is neutrally charged and DODAB is positively charged, DODAB and MO form cationic liposomes. DODAB:MO (1:2) liposomal systems are not toxic to cells (Oliveira 2016).

The net positive charge of DODAB:MO (1:2) formulation is favourable because cell membranes usually have slightly negative surface charge. The opposite charges may help the binding of the nanocarrier to the cell. Additionally, the neutral MO favours drug encapsulation within the liposome. The drug is encapsulated at inverted non-lamellar MO-enhanced phases inside of the vesicle. DODAB:MO liposomes have shelf life of about one month at 4 °C.

In the current commercial formulations, active loading techniques are used to precipitate DOX in the aqueous pool of the liposomes, highly increasing the drug content. This active loading mechanism, however, has raised some concerns about DOX dimerization and other toxic effects associated with the dimers, besides the smaller efficiency of DOX dimers to successfully intercalate within the DNA bases. The development of a new liposomal formulation, DODAB:MO liposomes, aims to increase the lipid content in comparison to the regular liposomes. Therefore, by possessing a lipid filled core rich in MO inverted structures the formulation proposes to increase the amount of DOX that can be loaded into the liposome by a passive loading technique, avoiding dimerization as well as provide a more stable drug delivery system. High concentration of DOX is able to partition in liposomes, the partition coefficient (K_p) at pH 5 of DOX in DODAB:MO (1:2) is reported to be 2818 (da Rocha 2014). The DODAB:MO (1:2) based nanocarriers show enhanced release in low pH medium indicating preferential release mechanism in cancer tissue (pH 5) compared to blood serum (pH 7.4) (da Rocha 2014).

To ensure that DODAB:MO (1:2) liposomes can be used as a nanocarrier system for the anti–cancer drug DOX, they have to be further characterised. Especially interesting is to know, where and how deep in the bilayer DOX is encapsulated, and to understand the uptake mechanism by performing *in vitro* cell studies to follow the time dependent intracellular distribution of DOX.

2.2 Doxorubicin (DOX)

DOX is a widely used, naturally fluorescent anthracycline antibiotic, anticancer drug. Although, the mechanism of action of DOX still remains unclear, two major mechanisms of intracellular cytotoxicity of DOX in cancer cells have been proposed:

1. Intercalation into DNA leading to the inhibition of DNA replication;
2. Production of reactive free radicals that results in DNA damage or lipid peroxidation (Thorn et al. 2012).

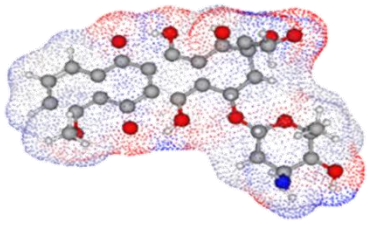

Figure 2. *Ball-and-stick model of DOX (blue - nitrogen, red - oxygen, white – hydrogen, grey – carbon) with surface charge distribution (red- polar zones, blue- non-polar zones). Created with software MarvinSketch 16.5.2* ©.

The active site of DOX is generally considered to be the nucleus of the cell. At physiological pH, DOX has positive charge, which favours intercalation with DNA by electrostatic binding to the negatively charged phosphate backbone (Drugbank.ca 2013). In addition, it inhibits the enzymes necessary for cell replication, leading to cell death. However, the lack of cell specificity and therefore risk of organ damage limits the maximum dose that can be safely prescribed, lowering the efficacy of the cancer therapy.

DOX is an amphiphilic molecule consisting of a hydrophobic tetracycline ring connected via a glycosidic bridge and a hydrophilic amino saccharide, the daunosamine (Figure 2). This pH-dependent feature allows DOX to be transported either in the internal aqueous core of liposomes or in its lipid membrane. DOX has three prototropic pK_a forms. DOX is an amphoteric molecule as the protonatable amino group of the sugar moiety (PK_{a1} = 8.15) gives basic features, while the deprotonation of phenolic rings (C11 with pK_{a2} = 10.16 and C6 with pK_{a3} = 13.2) give it acid characteristics.

DOX monomers have a major anti-tumour role while DOX dimers have less or no efficacy (Nakanishi et al. 2001). Dimerization of DOX in high concentrations can occur in either a parallel or antiparallel configuration.

2.2.1 Commercial liposomal formulation – Doxil®

Doxil® is a PEGylated liposomal formulation encapsulating DOX that was the first nanoengineered FDA-approved therapeutic, and is used as an effective cancer treatment medication for different types of cancers. Doxil® reduces the cytotoxicity of DOX by increasing the specificity and accumulation of DOX within the tumour site (Barenholz 2012). Nearly all liposomal medicines currently need to be injected intravenously as the liposomes will degrade in the digestive tract (Barenholz 2012). Doxil® liposomes are excreted from the body after several days, and the possibility of accumulation at sites

with a leaky vascular system is increased. Average liposome size in liquid suspension is reported to be about 90 nm (Bao et al. 2004). Surface-bound methoxypolyethylene glycol molecules covering the phospholipid bilayer, a process known as PEGylation, protect the liposomes from being detected by the mononuclear phagocyte system. This is a passive targeting strategy (Barenholz 2012).

Several new liposomal formulations have been proposed for the delivery of DOX (Silva et al. 2011; Neves Silva et al. 2014; da Rocha 2014). Majority of them uses "active loading" methods and a minority that use "passive loading" methods that achieve small encapsulation efficiencies of the drug. The "active loading" method allows encapsulating more DOX in liposomes, but it has the drawback of drug precipitation and formation of dimers. In case of Doxil®, liposomes are loaded with DOX HCl by the ammonium sulphate gradient technique. DODAB:MO liposome formulation (Neves Silva et al. 2014), enable increased amount of DOX, that can be loaded into a liposome without dimerization.

2.3 Cell interaction with liposomes

Cellular uptake studies can provide a better understanding of interaction between developed liposomes and cells. Based on that, liposomal formulations can be further optimized in order to enhance effectiveness and smart drug delivery.

Several liposome-cell interaction mechanisms have been reported in literature:

- Adsorption, release of content;
- Adsorption, transfer of lipophilic compound;
- Fusion;
- Endocytosis (Silva et al. 2012; Ducat et al. 2011; Kamps & Scherphof 2003).

Figure 3 schematically depicts endocytosis of pH-sensitive liposome (Shukla 2016).

Endocytosis is the most widely accepted cell internalization mechanism for liposomes, but it is possible that several pathways occur in parallel. This could be explained by the fact that specific cell lines prefer a particular mechanism of internalization but can use more than one mechanism.

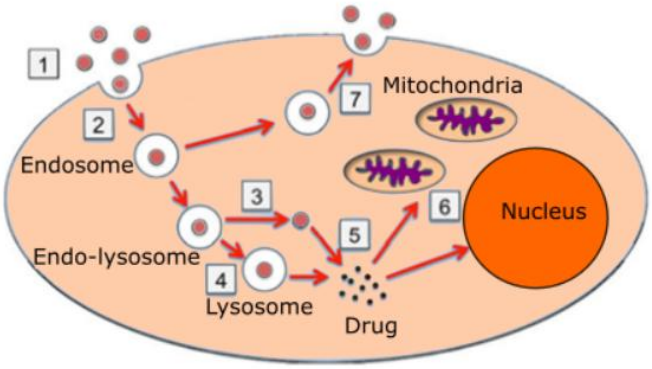

Figure 3. *Scheme of the endocytosis pathway of pH-sensitive liposomes. The relevant interaction mechanisms are illustrated: 1 - cellular association of liposomes; 2 - liposome in early endosomes; 3 - destabilization of endosome membrane and release of contents by pH-sensitive liposomes or 4 - lysosomal degradation; 5 - therapeutic agent fuses into cytoplasm; 6 - transport of therapeutic agent to the target; 7 – exocytosis, adapted from: (Shukla 2016).*

Mechanisms of liposome-cell interaction depend on the size, type and the composition of the liposomal formulation but also on the cell type and cell-cycle phase. Due to this, it is beneficial to study the cellular uptake of a specific liposome on more than one cell line. In this thesis, A431 (epidermoid carcinoma) and A549 (lung cancer) (Figure 4) human cell lines were used to assess the cellular uptake of DODAB:MO encapsulating DOX.

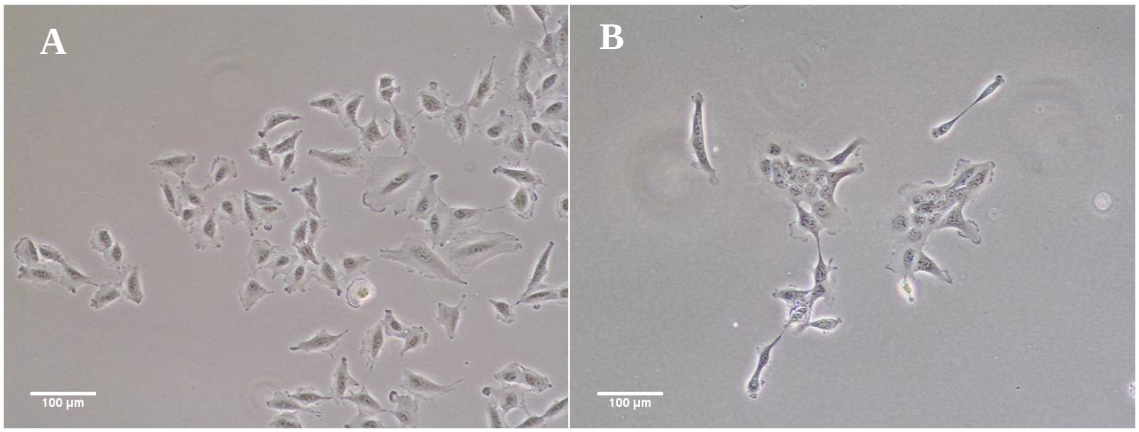

Figure 4. *Bright-field microscopy images taken with a Nikon Ti, Eclipse microscope of the cell cultures used for confocal imaging: A549 (A) and A431 (B) showing cells without introduction of liposomes.*

Untreated A549 cells are triangle shaped with wide and flattened cell morphology as can be observed in the bright-field microscope images taken to confirm proper cell growth during cell culturing (Figure 4 A).

A431 cells are derived from 85 years old female patient with epidermoid carcinoma. This cell line has high expression of epidermal growth factor receptor (EGF) (ATCC

n.d.). Doubling time for this cell line is between 25 and 30 hours (ATCC 2014). If A431 cells are stimulated with EGF it induces rapid tyrosine phosphorylation of intracellular signalling proteins, which control cell growth, proliferation and apoptosis (Graness et al. 2000). It has been reported that EGF reduces the resistance to DOX in A431 cell line (Kwok & Sutherland 1991). A431 cells are irregularly shaped, some individual cells tend to spread in spindle-like shapes but when colonies are formed cell shape changes to more compact irregular shape and they tend to grow in several layers, as can be seen in the bright-field microscope images taken during the cell culturing assay (Figure 4 B).

In vitro cell culture system experiments provide the opportunity to study liposome-cell interactions, by, for example, confocal laser scanning microscopy, fluorescence lifetime imaging microscopy and others. In addition, co-localization studies can be done of labelled particle components and dyes, or antibodies that recognize cell organelles or molecules playing a role in the process.

2.4 Suitable liposome characterization techniques

One of the most commonly used techniques to characterize liposomes are fluorescence-based techniques and their main advantage is possibility to monitor complexes' behaviour under physiological conditions (Madeira et al. 2011). The dynamic and electrophoretic light scattering (DLS and ELS) techniques are used for liposome size distribution determination and surface charge (potential zeta) determination, and a fluorescence quenching method for nanoscale localization of the drug inside the liposome formulation. FRET analysis allows to measure distances between fluorescent probes with sensitivities below 10 nm. In addition, microscopy methods such as atomic force microscopy and transmission electron microscopy can be used to assess macroscopic structure of liposomes (Madeira et al., 2011). For cellular uptake studies, laser scanning confocal microscopy has advantages of high resolution and ability to obtain information in three dimensions (3D).

2.4.1 Dynamic Light Scattering (DLS)

DLS is a well-known technique for measuring the size and size distribution of molecules and particles in suspension. Brownian motion is the unsystematic movement of particles, which is the result of collisions with the solvent molecules that surround them. The speed of these particle movements is used to determine particle size (Malvern Instruments 2000; Malvern Instruments 2013)

The speed of Brownian motion depends on the particle size, solvent viscosity and temperature. The bigger the particle is, the slower it moves, the higher the temperature is, the more rapid Brownian motion becomes. The laser light passing through the sample is scattered by the diffusing particles. The mean velocity of the Brownian motion relates

to the translational diffusion coefficient, which can be used to determine a particle size using the Stokes-Einstein equation (Malvern Instruments 2000; Malvern Instruments 2013).

2.4.2 Electrophoretic Light Scattering (ELS)

ELS can be used to measure the ζ-potential of the particles and it is used to characterize the stability of colloidal dispersions. The ζ-potential indicates the degree of electrostatic repulsion between neighbouring, similarly charged particles in dispersion. For small particles, high ζ-potential indicates stability – particles in the suspension will resist aggregation. When the potential is relatively small, the absence of charge repulsion may cause particle's flocculation. Particles with ζ-potentials higher than +30 mV or lower than -30 mV are normally considered stable.

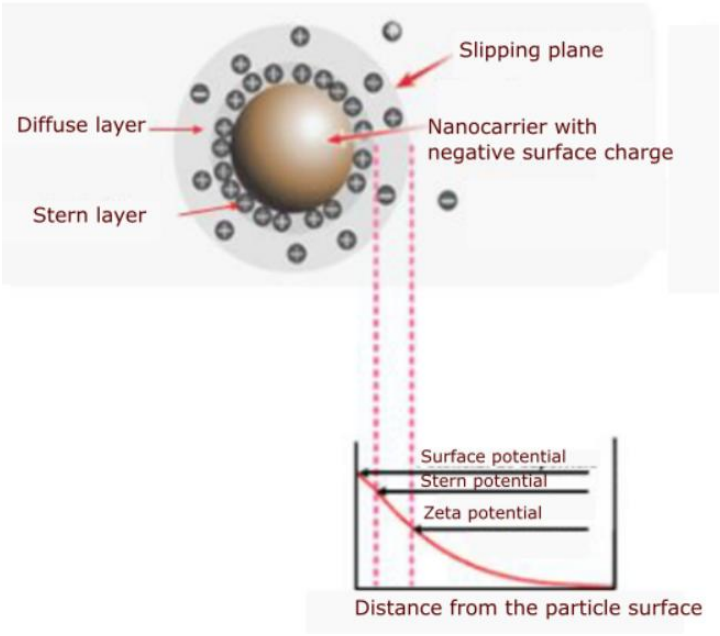

Figure 5. *Diagram showing the ionic concentration and potential difference as a function of distance from the charged surface of a particle, adapted from (Malvern Instruments 2013)*

Ions that are in the liquid surrounding the suspended particles are attracted to their surface if they have an opposite charge. The net charge at the particle surface determines the distribution of ions in the surrounding interfacial region, resulting in an increased concentration of counter-ions close to the surface. Liquid surrounding the particle can be described as electric double layer: closer to the particle, called the Stern layer, where the ion binding strength is strong, and further, a diffuse layer, where ions are less strongly bonded (Figure 5). There is a theoretical boundary in the diffuse layer where the ions and particles are stable. These ions, which are within the boundary, move with the particle. But any ions beyond the boundary are independent from the particle. This

boundary is called the slipping plane and the potential at slipping plane is the ζ-potential.

ELS experiments consist on applying a potential difference to a capillary, where the sample flows. Then the charged particles move to the poles of opposite charge and the velocity of the particles is measured using Laser Doppler Velocimetry, from which electrophoretic mobility is obtained. From the electrophoretic mobility and by application of the Henry equation it is possible to determine the ζ-potential of the particles (Malvern Instruments 2000).

2.4.3 Nanoscale drug localization

The target site of DOX is the cell nucleus where it is presumed that the drug binds to nucleic acids by specific intercalation (Drugbank.ca 2013). Therefore, DOX-loaded liposomes have to interact first with enzymes and receptors at cell membrane level before delivering its content to the nucleus. Thus, the concentration and location of the drug in the liposomal bilayer is a relevant parameter describing its pharmacologic and toxic effects. Elucidating the drug location/concentration at the lipid nanocarrier could contribute to optimize formulations with the ability to provide a controlled drug release to extend the therapeutic duration.

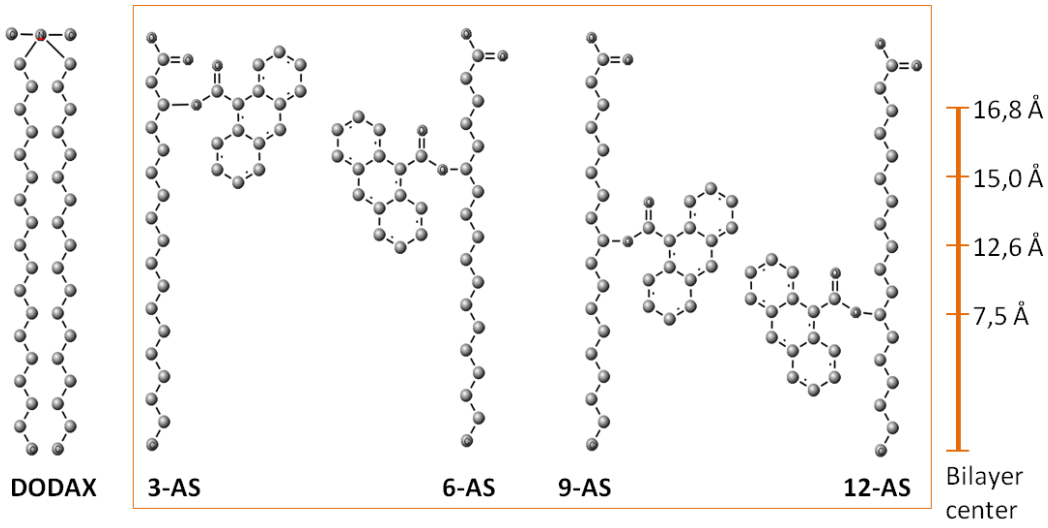

Figure 6. *Structure of DODAX (where X is counter ion) lipid, the AS-lipid with AS-dye attachment sites. Created with software MarvinSketch 16.5.2©.*

There are two types of methods to determine drugs' location in the membrane: direct and indirect. Direct methods include determination of localization by techniques like X-ray and neutron diffraction, nuclear magnetic resonance, infrared spectroscopy, and others (Mason et al. 1991). Indirect methods require a foreign compound that is usually a fluorescent probe, often referred to as molecular 'ruler'. The fluorescent probes used in this study are lipid molecules with fluorescent groups placed on varying specific lo-

cations of the acyl chain (see Figure 6). The fluorescent lipid probes are then inserted within the other lipid components of the liposomal formulation loaded with the drug. If a chosen property of the probes is altered, it is possible that these changes can be related to the localization of the drug.

For example, if the molecular location of a probe within membranes is known with certainty, the deactivation of the probe fluorescence (also known as fluorescence quenching) induced by a drug can be used to reveal the location of the drug inside the membrane.

For experiments in this thesis, probes with fluorescent groups on the 3rd, 6th, 9th and 12th carbon the acyl chain were chosen. The *n*-AS probes are inserted within the lipid components of DODAB:MO (1:2) vesicles and their lipid chains are aligned with the various carbon atoms along the carbon chain of DODAB (see Figure 6). The interactions between the fluorescent probe and DOX were studied using drug concentration-dependent spectroscopic quenching assays, that can be used to determine the static and dynamic Stern-Volmer constants. The most strongly quenched dye indicates the location, which is closest to the drug. The different optical spectroscopy methods used are described below.

2.4.3.1 Steady-state fluorescence quenching

Quenching can result from a variety of processes that decrease the fluorescence intensity.

In order to determine the amount of quenching, correction of the absorbance using the ratio of intensities of the steady state emission at the peak of each sample is necessary. The emission spectra allow to find the maximum fluorescence intensity values, which are then used to calculate quenching.

Absorbance inner filter correction is made using the Equation 1:

$$F_{correction} = \frac{1-10^{-A_0}}{1-10^{-A_t}} \cdot \frac{A_0}{A_t}, \quad (1)$$

where A_0 is the absorbance value of the system without quencher at chosen wavelength and A_t is the absorbance value of the system with increasing concentrations of quencher at chosen wavelength. Fluorescence emission is corrected by the use of Equation 2:

$$I_0 = F_{correction} \cdot \frac{I_f}{I_t}, \quad (2)$$

where I_f is maximum intensity value of the system without quencher and I_t is maximum intensity value of the system with increasing concentrations of quencher at chosen wavelength. One or more quenching mechanisms can occur in a system depending on its properties. Collisional or dynamic quenching is due to collisions between quenching

agents and fluorophores. The dynamic quenching molecule provides a non-radiative route for loss of the excited state energy and return to ground state. In static quenching the quenching agent forms a non-fluorescent complex with the quenching agent before the excitation occurs. The fluorophore and quencher have to be in contact for static and dynamic quenching (Lakowicz 2006b).

It is expected that the closer the DOX and the probes are physically, the stronger the quenching and therefore the larger decrease in steady-state fluorescence and/or lifetime (Lakowicz 2006b) .

Static and dynamic quenching can be distinguished by fluorescence lifetime measurements (which require instruments capable of time resolutions in the nanosecond range), and if the quenching process has a dynamic nature an equivalent decrease in fluorescence emission intensity and lifetime will occur:

$$\frac{I_0}{I} = \frac{\tau_0}{\tau} \ , \tag{3}$$

where I_0, I and τ_0, τ are the measured fluorescence intensities and fluorescence lifetimes of the fluorophore in the absence and presence of the concentration of the quencher.

The effective concentration of the quencher in the lipid membrane $[Q]_m$ can be calculated using equation:

$$[Q]_m = \frac{K_p \cdot Q_t}{(K_p \cdot Q_t) + (1 - V_m)} \ , \tag{4}$$

where K_p is partition coefficient of the drug, Q_t concentration of the drug added (in M) and V_m is the volume of lipid in membrane (Lakowicz 2006a).

In case of collisional quenching the graphical representation of the values of fluorescence intensity ($\frac{I_0}{I} - 1$) or lifetime ($\frac{\tau_0}{\tau} - 1$) as a function of $[Q]_m$ of the drug shows linear behaviour with a slope that corresponds to the Stern-Volmer constant (K_{SV}) that in this case is also called dynamic constant (K_D).

In a static quenching mechanism, fluorophore and drug form a complex that is non-fluorescent and fluorescence that is detected corresponds to the fraction of non-complexed fluorophores. Thus, in a static quenching, the fluorophores that are bound with the drug are undisturbed and the lifetime of the excited state remains constant:

$$\frac{\tau_0}{\tau} = 1 \tag{5}$$

Linear Stern-Volmer plots do not prove that dynamic quenching of fluorescence has happened. Static quenching can result in linear plot as well. With fluorescence lifetime measurements it is possible to determine, which quenching process occurrs.

Non-linear Stern-Volmer plots with a downward curvature towards the x-axis may indicate that there is a mixture of fluorophores that are not exposed to the quencher together with fluorophores that are more accessible to the quencher. This negative deviation to Stern-Volmer linear plots is common in proteins that may contain several populations of intrinsic fluorophores. Indeed, proteins can contain tryptophan, tyrosin and phenylalanine residues that act as fluorophores and are positioned in distinct environments. Stern-Volmer plots for these proteins frequently curve downward, reflecting the quenching of the accessible fluorophore, only.

Non-linear Stern-Volmer plots with an upward curvature can occur when the extension of quenching is high and can be due to uneven distribution of either the quencher and/or the fluorophore. Combined static and dynamic quenching and the sphere-of-action model can explain positive deviations from linear Stern-Volmer plots:

1. Combined static and dynamic quenching

In many cases the fluorophore can be quenched both by collisions and by complex-formation with the same quencher, traduced by the following equation:

$$\frac{I_0}{I} - 1 = (K_D + K_S)[Q]_m + K_D K_S [Q]_m{}^2, \quad (6)$$

where K_D and K_S are respectively the Stern-Volmer constants for dynamic and static quenching.

2. Sphere-of-action model

Positive deviations from linearity in the Stern-Volmer plot are also frequently observed when the extent of quenching is large, and it happens when the quencher is close to the fluorophore at the moment of excitation. The modified form of the Stern-Volmer equation that describes this situation is:

$$\frac{I_0}{I} = (1 + K_D[Q])e^{[Q]V_{app}}, \quad (7)$$

where V_{app} is the apparent volume of the sphere adjacent to the fluorophore where there is higher probability to find the quencher at the time of excitation. This volume can be calculated by:

$$V_{app} = V_{sphere} \cdot \frac{K_p}{1 + K_p \cdot V_m}, \quad (8)$$

where V_{sphere} is the additive volume of the quencher and the fluorophore.

2.4.3.2 Time-Correlated Single Photon Counting (TCSPC)

To determine fluorescence quenching of the AS probes in the presence of DOX, fluorescence lifetime spectroscopy, specifically time correlated single photon counting (TCSPC), can be used. With this method a deeper understanding of the liposomal formulation can be obtained.

TCSPC is a technique used for measuring the fluorescence decay times in ranges starting from picoseconds and above. It is intended for samples with exceptionally small concentrations of fluorophores. High sensitivity and accuracy with picosecond time resolution are the advantages of TCSPC.

The principle of TCSPC is based on the detection of single photons and the measurement of their arrival times with respect to a reference signal. Samples are excited using a pulsed light source to achieve data collection of the arrival times of the individual photons over many excitation cycles. Then decay curves are constructed from many individual time measurements (Wahl 2014b).

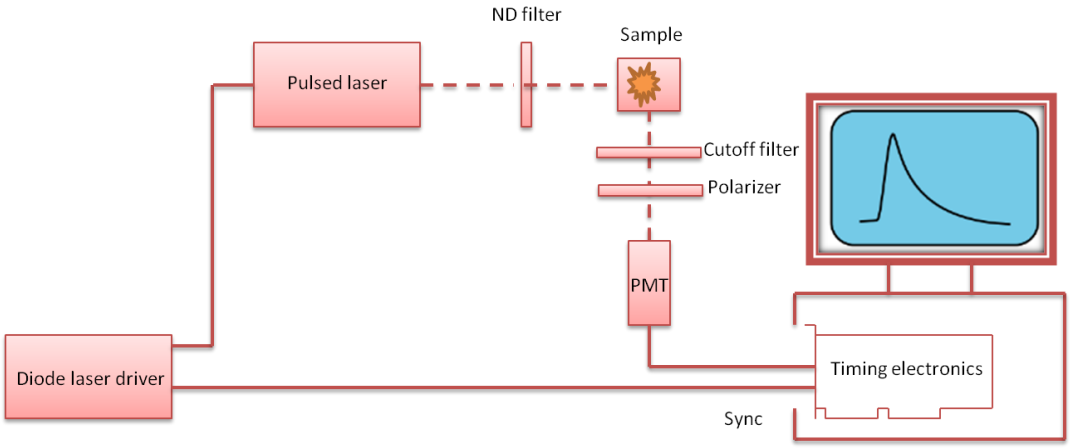

Figure 7. *Adapted experimental set-up for fluorescence decay measurements with TCSPC. Adapted from (Wahl 2014a).*

Figure 7 shows a schematic set-up for fluorescence lifetime measurements with TCSPC. The picosecond diode laser is running on its internal clock. The driver box is separate from the actual laser head, which is attached with a flexible lead. The light pulses of typically 50 ps are directed at the sample cuvette through appropriate optics. A neutral density filter is used to attenuate the light levels to maintain single photon statistics at the detector.

Upon excitation, the fluorescent sample emits light at a longer wavelength than that of the excitation light. The fluorescence light is filtered out against scattered excitation light by means of an optical cut-off filter. A polarizer is placed in front of the photomultiplier tube (PMT) detector and oriented at the magic angle 54.7 degrees, with respect to the linear polarization of the laser excitation beam. The light then is detected and ampli-

fied PMT. The electrical signal obtained from the detector is fed to the TCSPC electronics. The laser driver also provides the electric synchronization signal (SYNC) needed for the photon arrival time measurement (Wahl 2014a). Figure 8 illustrates how time differences between the excitation and the photon detection are measured by electronics that act like a stopwatch (Wahl 2014a). The histogram of photon arrival times with respect to laser excitation pulses are formed over multiple cycles.

Figure 8. *Measurement principle of start-stop times in time-resolved fluorescence measurement with TCSPC, diagram adapted from* (Wahl 2014a).

TCSPC is statistical method and high repetition pulsed laser sources are required in order to accumulate sufficient amount of photon events for certain precision. The probability of registering more than single photon per cycle needs to be low. With TCSPC only the first photon within one laser repetition period is observed. Consequently, several photons cannot be detected if operated at too high intensities. Therefore the intensity has to be low such that typically in many cycles no photon is registered (Wahl 2014b). The detection rate used in the described measurments in this thesis was 1 photon per 1000 000 excitation pulses. The time is measured between the excitation pulse and the observed photon and stored in a histogram.

The difference in the amount of time it takes for an absorbed photon to be re-emitted gives useful information about the sample. Fluorescence lifetime of the *n*-AS probes could be dependent on their interactions with the DOX, as DOX is capable of taking up some of the energy from the probe, leading to a faster photon re-emission from the probe. Fluorescence dynamics typically can be characterized by a multi-exponential decay:

$$x(t) = \sum_{i=1}^{M} A_i \cdot e^{-t/\tau_i}, \tag{9}$$

where A_i denotes the amplitude and τ_i the decay times of the M exponential components of the fluorescence decay.

The instrument response function (IRF) is measured once before all TCSPC measurements were performed to summarize TCSPC system's overall timing precision. Usually one of the weakest timing components in TCSPC system is the detector. The accuracy of timing is limited by the conversion from a photon to an electrical pulse by the detec-

tor. Another weak component of the system is the excitation source - it can broaden the IRF curve. Thus, a short 50 ps pulsed laser is used.

Analysis of the fluorescence decay data includes appropriate mathematical fitting and deconvolution in order to account for the IRF and to calculate fluorescence decay for each sample.

2.4.4 Förster Resonance Energy Transfer (FRET)

Quenching requires molecular contact between the fluorophore and quencher. The amount of quenching is sensitive to molecular factors that affect rate and probability of contact due to short interaction distance. FRET on the other hand occurs up to distances of about 10 nm between FRET partners, which are fluorescent molecules with a suited spectral overlap and relative molecular orientation.

FRET describes mechanisms in which a decrease of the intensity of fluorescence of one species acting as donor is due to transference of the energy to an acceptor. In collisional quenching the emission intensity of initially excited molecule decreases regardless the acceptor being fluorescent or non-fluorescent. Comparison of FRET and quenching gives better understanding of the nature of both processes.

In quenching mechanisms, DOX will act as the acceptor and the probe will act as the donor, allowing energy to be transferred between the probe and DOX. While DOX itself is a fluorescent molecule, the spectra of the fluorescent markers on the *n*-AS-probes and DOX only allow the transfer of energy from the AS probes to the DOX, as the AS probes absorb higher energy photons than DOX. It is expected, that the closer the DOX and the probes are physically, the more efficient is the FRET process.

In the FRET mechanism the rate of energy transfer depends upon i) the extent of spectral overlap of the emission spectrum of the donor (AS probes) with the absorption spectrum of the acceptor (DOX), ii) the quantum yield of the donor, iii) the relative orientation of the donor and acceptor transition dipoles, and iv) the distance between the donor and acceptor molecules. The distance dependence of FRET allows measurement of the distances between donors and acceptors.

The transfer efficiency (E) is the fraction of photons absorbed by the donor that are transferred to the acceptor and is given by:

$$E = \frac{{R_0}^6}{{R_0}^6 + {r_{DA}}^6}, \tag{10}$$

where $r_{D\text{-}A}$ is the distance between donor and acceptor, R_0 is the Förster distance, which is the distance at which FRET is 50% efficient. From Equation (11) it is possible to calculate the distance between donor and acceptor:

$$r_{DA} = R_0 \sqrt[6]{\frac{1-E}{E}}. \quad (11)$$

E is typically measured using the relative fluorescence intensity of the donor, in the absence (I_D) and presence of the acceptor (I_{DA}):

$$E = 1 - \frac{I_{DA}}{I_D}. \quad (12)$$

The Förster distance can be calculated by:

$$R_0 = 0{,}211(k^2 n^{-4} Q_D J(\lambda))^{1/6}, \quad (13)$$

where k^2 is a factor describing the relative orientation in space between the transition dipoles of the donor and acceptor, n is the refractive index of the medium, Q_D is the quantum yield of the donor in the absence of acceptor, and J(λ) is the overlap integral in the region of the donor emission and acceptor absorbance spectra (with the wavelength expressed in nanometers).

Often the observation of FRET is enough to identify binding events, even without calculation of the D–A distance, as FRET is limited to short distances of about 10 nm. From comparison of the distance for FRET with the size of the molecules, one can see that FRET is a through-space interaction.

2.5 Cellular uptake study techniques

For cellular uptake studies, fluorescence microscopy techniques were considered because of DOX's fluorescence properties. DOX has wide excitation (450-550 nm) and emission (525-650 nm) spectra (see results from the spectroscopic studies presented in Figure 16 and 22).

Confocal microscopy has several advantages over conventional optical microscopy methods: depth of field is shallow, out-of-focus light is eliminated and it allows to optically section thick specimens (larger than 2 micrometers). Imaging of both fixed and living cells is possible. In addition, it is a method that can be adapted to investigate a broad range of systems by varying the excitation or detection wavelength range and fluorescent labels (Dailey 2016).

2.5.1 Confocal laser scanning microscopy

Confocal microscopy is a specialized technique of light microscopy and is a commonly used in cellular uptake studies. Either autofluorescent or samples stained with fluorescent markers are required in order to use this technique.

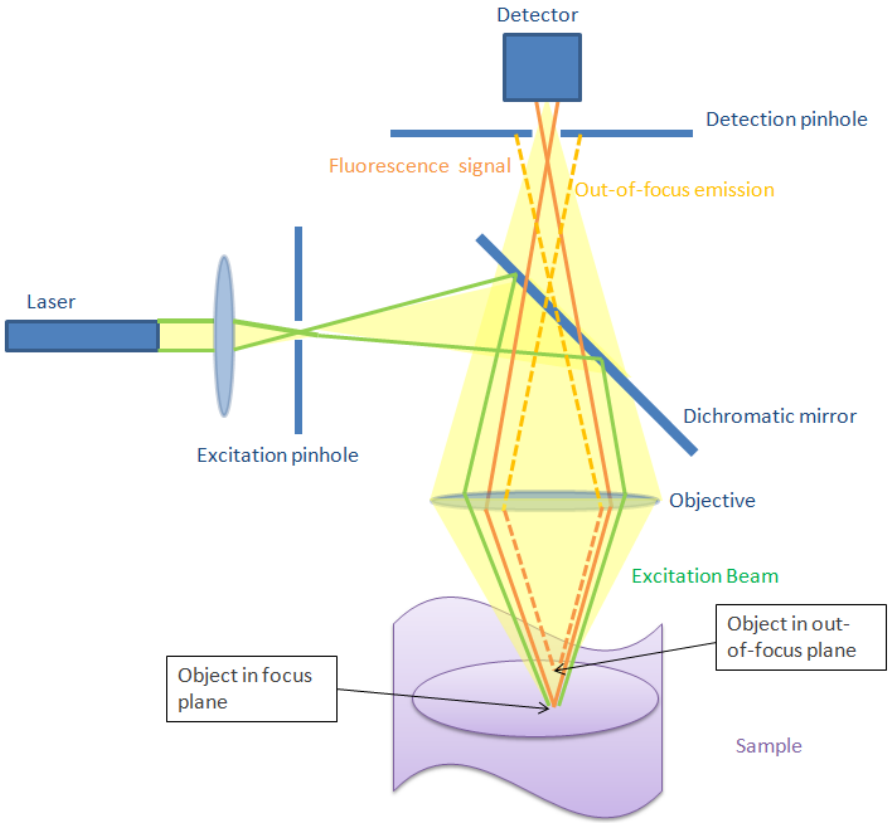

Figure 9. *Confocal principle based set-up geometry. The scheme shows effective blocking of out-of-focus emission by a pinhole that is placed in front of the detector and matched to let the fluorescence signal pass that originates from the focal volume, only. Adapted from (Fujimoto & Brezinsky 2003).*

Laser scanning confocal microscope (LSCM) designs are centred around upright or inverted optical microscopes. A laser system is used as a light source to excite fluorophores in the sample, signal information is delivered to a detector (photomultiplier tube or avalanche diode) and processed by a computer.

The principle of confocal microscopy is presented in Figure 9. Coherent excitation light emitted from a laser system passes through a pinhole aperture that is in conjugate plane with a focus point on the specimen and with a second pinhole aperture that is situated in front of a detector. Light is directed onto the sample of interest in a specific focal plane by a dichromatic mirror. The fluorescence emitted from the specimen in the same focal plane passes back through the dichromatic mirror and is focused onto the pinhole aperture. This pinhole allows the light originating from the focus to pass to the detector, while rejecting the majority of the light from out-of-focus planes. This way, the signal-to-noise ratio for the features of interest is increased (Fujimoto & Brezinsky 2003). To use this improved signal-to-noise ratio for high-contrast imaging, a laser scanning system is implemented into a confocal microscope setup.

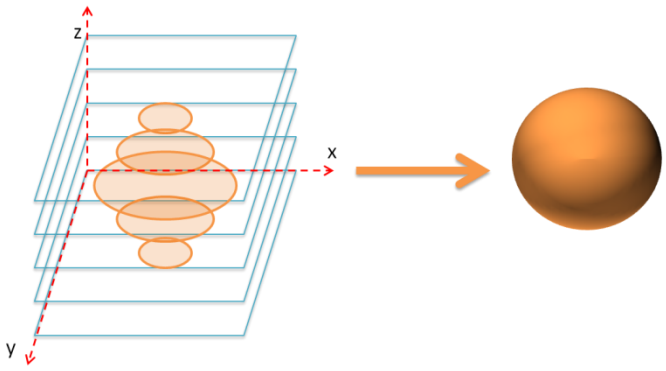

Figure 10. *Principle of z-stack image acquisition. After each 2D scan of the excitation laser in the xy plane, the sample is moved in z direction. This sectioning allows obtaining 3D images from objects (here a sphere), and can be used to investigate single biological cells.*

The image is built up on a pixel-by-pixel basis using the scanning mechanism. The scanning principle is represented in Figure 10: A focused light beam is scanned across a defined area in a raster pattern by two oscillating mirrors. One of the mirrors is used to move the beam from left to right across lateral x axis, while other translates it in y direction. After scan of x axis beam is moved to starting position and shifted along y axis. When information across x-y axis is collected, the position along the z-axis is changed and the process is repeated for a defined thickness.

The properties of visible light set limitations to the achievable resolution in confocal microscopy. Wavelength, properties of sample and restrictions of microscope optics result in the maximum resolution of about 200 nm. Thus, the minimum distance by which two objects can be detected from each other is 200 nm (Fujimoto & Brezinsky 2003). The size of liposomes is around 100 nm. Therefore, the precise structural information about one vesicle cannot be obtained by confocal microscopy but the accumulation of the fluorescent anti-cancer drug DOX around or inside the cells, which typically have diameters of around 10 to 30 μm can be studied.

3. RESEARCH METHODOLOGY AND MATERIALS

3.1 Liposome sample preparation

For spectroscopic characterization studies DODAB:MO (1:2) liposome samples were prepared containing 3-AS, 6-AS, 9-AS and 12- AS probes and 6 varying concentrations of DOX. And for cell internalization studies DODAB:MO (1:2) (DOX@DODAB:MO) liposome samples were prepared containing DOX in concentrations of 5 μM and 40 μM.

3.1.1 DODAB:MO (1:2) liposomes

Stock solutions of DODAB and MO (20 mM) were prepared by dissolving the lipids in ethanol. 117 μL of DODAB and 233 μL of MO stock ethanolic solutions were added to a glass tube and solvent was dried under a nitrogen stream with a constantly rotating motion to form a lipid film. Lipid films were hydrated with 7 mL ultrapure water. Film/water solution was warmed up above the lipid mixture T_m (60 ºC). A cycle of one minute of incubation in a warm water bath at 60 °C and one minute vigorous vortexing was repeated for 20 minutes until the whole lipid film was removed from the glass walls and the multilamellar vesicles had been formed.

Subsequently, extrusion process of the vesicles followed using a Northern Lipids Lipex Extruder and Nuclepore Track-Etch Membrane filters. The extrusion process uses air pressure to apply force to a liquid sample, pushing the sample through a filter with pores of the desired size and ensuring the particles in the sample are all uniform. The liposomes were extruded to ensure uniform size of about 100 nm. That was achieved by extruding the liposomes containing the necessary probe 5 times with a 400 nm filter, 5 times with a 200 nm filter and 10 times with a 100 nm filter. Extrusion protocol for liposomes for cell internalization studies was following: 2 times with a 400 nm filter, 2 times with a 200 nm filter and 10 times with a 100 nm filter.

The samples were stored in a fridge at a temperature of 6 °C until further analysis was performed.

3.1.2 *n*-AS@DODAB:MO

For spectroscopic characterization studies DODAB:MO (1:2) lipid films with probes were made by pipetting ethanolic stock solutions: 117 μL of 20 mM DODAB, 233 μL of 20 mM MO and 7 μL of 10 μM of *n*-AS (3-AS, 6-AS, 9-AS or 12-AS) probe into aluminium foil-covered glass tubes. Aluminium foil was used to avoid bleaching of the light-sensitive probes.

After collecting ingredients in desired ratio a drying process to form lipid films was performed. Then lipid films were hydrated with 7 mL ultrapure water. Film/water solution was warmed up above the T_m (60 ºC). A cycle of one minute of incubation in a warm water bath at 60 °C and one minute vigorous vortexing was repeated for 20 minutes until the whole lipid film was removed from the glass container and the multilamellar vesicles had been formed. Subsequently, the vesicles were extruded to achieve the desired size and homogeneity (described in Section 3.1.1).

3.1.3 DOX@DODAB:MO

After the extrusion process, the liposomes were loaded with DOX. Depending on desired experiment with or without *n*-AS probe and varying concentrations of DOX.

For quenching studies *n*-AS labelled DODAB:MO(1:2) liposomes were combined with DOX at concentrations ranging from 0 μM to 100 μM (0 μM, 20 μM, 40 μM, 60 μM, 80 μM, 100 μM). The samples were then incubated in a 37 °C water bath for 60 minutes to allow incorporation of the drug into the liposomes.

For cell uptake studies DODAB:MO(1:2) liposomes without *n*-AS probes were loaded with 5 μM and 40 μM DOX. Samples´ incubation in a 37 °C water bath for 60 minutes followed to allow incorporation of the drug into the liposomes. After incubation liposomes were diluted 1:10 in warm (37 °C) Dulbecco's Modified Eagle Medium (DMEM).

3.2 Experimental setup for liposomal characterization studies

For liposomal characterization the following methods were used: DLS, ζ-potential experiment, fluorescence quenching assay, and FRET analysis.

Temperature of 40 °C for all measurements was chosen to be at liquid-crystalline phase for the liposomal formulation and above phase transition.

3.2.1 Dynamic Light Scattering (DLS)

A volume of 1 mL of DODAB:MO (1:2) sample was placed in a 3 mL disposable polystyrene cuvette. The DLS instrument Malvern Zetasizer Nano ZS particle analyser was used to measure the mean diameter, its respective standard deviation and the polydispersity index (PdI) (Malvern Instruments 2013). 5 runs were performed with parameters presented in Table 1.

Table 1. *Parameters used for DLS particle size determination*

Material Refractive index Absorption	Polystyrene latex 1.590 0.01
Dispersant Temperature Viscosity Refractive index	Water °C 0.8872cP 1.330
Dispersant viscosity is used as sample viscosity	
Temperature Equilibration time	25.0 60 seconds
Cell type	Disposable sizing cuvette
Angle of detection Measurement angle	 170°
Measurement Number of runs Run duration Number of measurements Delay between measurements	 5 80 seconds 1 0
Positioning method Automatic attenuation selection Analysis model	Seek for optimum position Yes General purpose (normal resolution)

The PdI is dimensionless and scaled number that is calculated using the cumulants analysis. It is related to the peak width of the size distribution graph and shows if measured sample suspension is mono- or polydisperse. According to Malvern, samples with PdI values between 0.05 (highly monodisperse) and 0.7 (broad size distribution) are suitable for the DLS technique (Malvern Instruments 2000).

For soft materials (such as liposomes) it is unlikely to reach these values. In this particular case, where a combination of two lipids is used, it is even more difficult to reach a very low PdI. However, values of lower than 0.2 were considered as acceptable for a homogeneous size distribution.

For particle size measurement Malvern Zetasizer Nano ZS gives the result as an intensity particle size distribution (PSD) and these results are shown in this thesis. However, the number distribution was also considered to see if one or several intensity popula-

tions with distinct sizes are present in the sample solution. By the analysis of the particle size histogram it is possible to elucidate the number and relative percentage of each population.

3.2.2 Electrophoretic Light Scattering (ELS)

For ELS experiments, a clear disposable folded capillary zeta cell was filled with 1mL of sample and placed in a Malvern Zetasizer Nano ZS analyser. Measurement of 5 runs was performed, the parameters used are shown in Table 2. The ζ-potential obtained gives information about the liposome surface charge, which cannot be measured directly. The liposome surface charge determines the tendency of the nanoparticles to aggregate, furthermore it allows to estimate the formulation's shelf stability.

Table 2. *Parameters used to measure the zeta potential*

Material Refractive index Absorption	Polystyrene latex 1.590 0.01
Dispersant Temperature Viscosity Refractive index Dielectric constant	Water 25°C 0.8872cP 1.330 78.5
F(Ka) selection F(Ka) value Dispersant viscosity is used as sample viscosity	Smoluchowski 1.50
Temperature Equilibration time	25.0 60 seconds
Cell type	DTS1060C – Clear disposable zeta cell
Measurement Number of runs Number of measurements Delay between measurements	 5 1 0 seconds
Automatic voltage selection Automatic attenuation selection Analysis model	Yes Yes Auto

3.3 Nanoscale drug localization studies

For nanoscale drug localization studies fluorescence steady state emission, absorption and fluorescence lifetime spectra were recorded for *n*-AS labelled DODAB:MO(1:2) liposomes containing DOX in varying concentrations. The experimental parameters and used set-ups are described in the following sections.

3.3.1 Steady-state fluorescence spectroscopy

The steady state spectroscopy measurements were performed on a Horiba Scientific FluoroMax-4 spectrofluorometer. The cuvettes with volume of 1 mL of each sample were placed in the spectrofluorometer. Samples analysed were DODAB:MO (1:2) liposome samples labelled with one *n*-AS probe (where *n* is 3, 6, 9 or 12) and varying DOX concentrations 0 μM, 20 μM, 40 μM, 60 μM, 80 μM and 100 μM (Figure 17).

The chosen experiment type was spectral acquisition. The excitation wavelength was set to 379.00 nm and the emission spectra recorded was from 385.00 to 700.00 nm, with increment of 1 nm. Integration time per spectrum was 0.1 s. Front entrance and exit slits were set to 2.00 nm slitwidth. The grating had a line density 1200 l/mm. Before starting each acquisition a 5 minutes waiting period was set for temperature stabilization. Emission spectra were recorded once for all 24 samples.

3.3.2 Ultraviolet-visible spectrophotometry

The UV-VIS measurements were performed on a Perkin Elmer Lambda 950 UV-VIS spectrometer. UV-visible absorbance of each sample was measured between 300 nm and 450 nm. To reduce the signal-to-noise ratio, the scan speed was set to ‘slow’ and the slit width was set to 2.0 nm.

Before measuring the samples, absorbance spectrum of the solvent (MilliQ) water was recorded with the same settings. This was done for background correction purposes. Samples analysed were DODAB:MO (1:2) liposome samples labelled with one *n*-AS probe and varying DOX concentrations 0 μM, 20 μM, 40 μM, 60 μM, 80 μM and 100 μM (Figure 18).

3.3.3 Fluorescence Lifetime Spectroscopy

Fluorescence lifetime spectroscopy was performed using a ChronosBH spectrometer from ISS Inc. The measurements were performed for liposomal DODAB:MO (1:2) samples with 3-AS, 6-AS, 9-AS and 12-AS probes and 6 different DOX concentrations. Each measurement was repeated 5 times.

In this thesis ISS ChronosBH fluorescence lifetime spectrometer with Hamamatsu picosecond light pulser PLP-10 exciting at 379 nm wavelength with maximal 363 mW average laser power and 50 ps pulse duration was used at a repetition rate of 10 MHz.

A Semrock OD 0.03 filter was placed in front of the sample and a Semrock BP 435/40 filter was placed in front of the detector to only allow light of 415 to 455 nm to reach the detector. As DOX is excited at 480 nm and emits around 590 nm, the filter blocks all fluorescence from DOX and only detects photons from the fluorescence of the AS

probes. The broadband polarizer in the detection path was set to 54.7 degrees, or the magic angle, and each measurement was taken with 20s acquisition time. The laser position was adjusted to achieve maximum intensity and to ensure that there was no reflection occurring that could re-excite the sample and cause incorrect results. The detector was a PMT from Hamamatsu (H7422-40). Each sample was measured in a 2 mm glass cuvette. The IRF was measured a 2 mm cuvette filled with MilliQ water, and the Bandpass filter was removed, to let the scattered laser light pass to the detector.

3.4 Förster Resonance Energy Transfer (FRET)

Full fluorescence emission spectra recorded with an excitation wavelength of 379 nm and a detection range from 385.00 to 700.00 nm in a Horiba Scientific FluoroMax-4 spectrofluorometer were considered for the analysis of FRET between *n*-AS probes and DOX in the various DODAB:MO (1:2) liposomal formulations. The experimental setup described in Section 3.3.2 was used.

3.5 Cell samples

Fixed A431 and A549 cell samples were prepared for experiments, additionally A431 cell samples were prepared for live cell imaging.

3.5.1 Cell culture assay

Human carcinoma cell lines A431 and A549 cells were provided by Prof. Andreia Gomes from University of Minho (Braga, Portugal).

A431 (epidermal carcinoma cell line) and A549 (lung carcinoma cell line) cells were grown in 75-cm^2 flasks (BD Falcon, Franklin Lakes, NJ) with 12 mL of Dulbecco's Modified Eagle's Medium (DMEM) with 4.5 g/L glucose (Gibco® USA) supplemented with 10% Fetal Bovine Serum (FBS) (Gibco® USA), and 1% strep/pen (Penicillin (10,000 IU/mL), streptomycin (10,000 μg/mL)), which will be further referred to as "cell culture medium" (Gibco® USA). Cell handling was done under laminar flow hood and samples were kept in an incubator at 37°C with atmospheric CO_2 concentration of 5%.

Subculturing was done respecting the American Type Culture Collection (ATCC) recommendations for both cell lines. Before plating, cells were washed with 5 mL of 1X Phosphate-Buffered Saline (PBS) (Sigma-Aldrich, USA) to remove all traces of serum that contains trypsin inhibitor. When PBS was removed, 2 mL of 0.25% trypsin EDTA (Gibco® USA) solution was added and cells were incubated in 37°C for 5 minutes. When cells were well detached 3 mL of cell culture medium was added and aspirated by gentle pipetting.

Then cells were counted using a Newbauer hemocytometer after being diluted 1:1 in Trypan Blue counting solution to exclude dead cells, which stain blue. The number of cells per mL of cell suspension was calculated knowing the volume of the counted area and the dilution factor.

For new culture vessels in 75-cm^2 flasks aliquots of 250 000 cells of the cell suspension were added to cell culture medium with total volume of 12 mL. Cells were passaged every 7 days and medium was changed every 2-3 days.

3.5.2 Fixed cell samples

For cell uptake studies A431 and A549 cells were plated at a density of 100,000 cells/mL in an ibidi 8 well µ-slide (ibidi, Martinsried, Germany) one day prior to imaging. 200 µL of the $1x10^5$ concentration of cells were added to each well. The bottom of the µ-slide is glass coverslip no. 1.5H- suitable for microscopy. After incubating for 24 hours in a µ-dish, the cell culture medium was removed from each well and was replaced with 200 µL of either 5 µM free DOX, 5 µM DOX@DODAB:MO, 40 µM DOX@DODAB:MO, all in cell culture medium, or diluted (1:80) commercial liposomal formulation Doxil®. It was ensured that suspension added to cells contained less than 10% of water as higher water content might induce cell death. A control sample of cells left without suspension containing the drug was prepared in one of the wells. At different time points (1, 2, 4 and 6 hours) after introduction of different suspensions containing DOX, these solutions were removed and cells were washed with PBS. When PBS was removed, 200 µL of a 4% Paraformaldehyde (PFA) (Sigma-Aldrich, USA) solution in PBS was added for 20 minutes, then PFA was removed washed two times with PBS and 50 µL (2 drops) of VECTASHIELD® (Vector Labs, Burlingame, USA) mounting medium was added.

3.5.3 Live cell samples

For live or living cell experiments the A431 cells were incubated for 24 hours to allow cells to adhere and grow till confocal imaging was performed. For visualization of DOX uptake in live A431 cells, a nucleus staining fluorescent stain Hoechst 33342 (1:2000, molecular probes, Life Technologies, Eugene, USA) was used with incubation time 10 minutes.

After incubation and staining cells were gently transferred to the stage top incubator system (okolab) in the LSCM where a temperature of 37°C and 5% CO_2 environment was maintained. When the LSCM system was set and ready for experiment medium was removed before adding 200 µL of 5 µM or 40 µM DOX@DODAB:MO in cell culture medium. When solution containing DOX was added live cell experiment started.

3.6 Cell uptake studies of liposomes

Cell uptake studies for fixed and live A431 and A549 cells were done using confocal laser scanning microscopy.

3.6.1 Confocal laser scanning microscopy

Confocal microscopy was performed with a Zeiss LSM 780 confocal microscope (Carl Zeiss Microimaging GmbH, Jena, Germany). For live cell imaging, okolab incubator with temperature and CO_2 control was utilized. ZEN 2009 software (Carl Zeiss Microimaging GmbH) was used for image acquisition and Fiji/ImageJ software (U. S. National Institutes of Health, Bethesda, Maryland, USA) for image processing and 3D rendering.

For fixed cell uptake studies a 40x times objective (EC PlanNeoFluar 40x/1.3 NA Oil immersion, Zeiss) was used. For live cell imaging a higher magnification of 63x (Plan Apo 63x/1.4 NA oil immersion, Zeiss) was chosen. Live individual cells were selected for a time-dependent observation of the interaction of a cell with the anti-cancer drug DOX loaded DODAM:MO liposomes.

Each sample was imaged simultaneously with both the confocal and transmission mode. The transmission images are used to follow the cell shape and location changes, that allow deducting the cell cycle state. The confocal images are used to determine the location of the DOX within the cells. 353.55µm*353.55µm images with 512 x 512 pixels were acquired in the x, y plane. The z-stacks were measured moving the sample using a piezostage to move along the varying heights (25-50 µm) of the z-axis (with approximately 1 µm thick slices). Total number of slices was 25-50 slices. The z-stacks were measured at a variety of time points that were fixed after the incubation with DOX containing solutions (1, 2, 4 and 6 hours). Confocal images at varying z-heights were taken and combined to create 3D images of the cells. Acquisition time per pixel was 7.7 s and 488 nm laser intensity used was 0.7.

For the detection of DOX fluorescence a 488 nm laser was used for excitation and a band pass filter with transmission between 531 and 689 nm was placed in front of the detector. The fluorescence of the nuclear stain Hoechst 33342 was excited with 405 nm laser and a bandpass filter with transmission between 410-491 nm was placed in the epifluorescence detection channel.

4. DEVELOPMENT OF A FITTING LIFETIME ANALYSIS ALGORITHM

Fluorescence lifetimes were determined using the TCSPC technique. Two different fitting algorithms were examined in order to find the most appropriate one for measured data: commercial software Vinci Analysis by ISS for which several drawbacks were identified for the analysis of large sets of fluorescence lifetime curves and a new implementation of a fluorescence lifetime analysis tool that was developed in the frame of this thesis using Matlab software. Fitting algorithms were tested for data from DODAB:MO+9AS samples with different DOX concentrations.

4.1 Vinci Analysis by ISS

The principle of data analysis in the Vinci analysis software is to compare a model with the acquired data using a Levenberg-Marquardt algorithm as the minimization routine for the χ^2 -function. The model with the lowest value for the χ^2 -function is chosen for the system (ISS inc. 2015). According to ISS, Levenberg-Marquardt algorithm (LMA) was chosen because of its speed and stability (ISS inc. 2012).

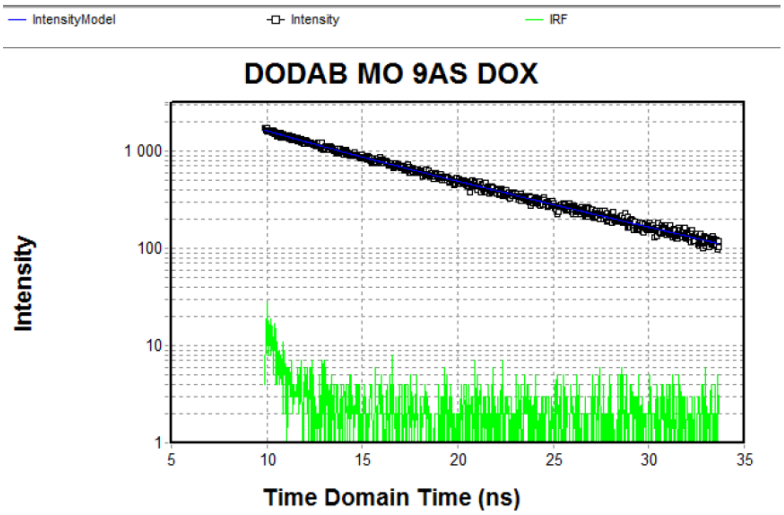

Figure 11. *Example of multi-exponential fitting with Vinci Analysis by ISS for DODAB:MO+9AS+20 µM DOX first iteration data*

LMA is a numeric minimization algorithm that solves non-linear least squares problems. These problems arise usually in least squares curve fitting. Initial guess for the parameters is needed to start the minimization. Levenberg-Marquardt curve-fitting

method is a combination of two minimization methods: the gradient descent and the Gauss-Newton method. Usually, a standard guess can be made even if it is far from final minimum, but in more complex cases the algorithm converges only if the initial guess is already close to the final solution (Gavin 2015). Vinci allows data analysis of decay times with more complicated models of up to 4 components. It is possible to analyse each component assuming a lifetime distribution (Planck, Uniform, Gaussian, Lorentzian).

There are several drawbacks, when using the Vinci Analysis by ISS, firstly, only limited information about commercial software's actual algorithm is available, therefore it can be classified as 'black box' analysis. Secondly, only one dataset at a time can be analysed. And, lastly, software needs manual input of initial decay times and desired time range by two clicks of mouse in plot- nearly impossible to repeat it for each dataset with the same precision. In addition, author observed inconsistencies in outputs when the fitting was repeated for the same sample several times. The reports from Vinci Analysis can be exported in MS Word or PDF format thus are not ready for further analysis.

All measured data was processed with Vinci Analysis by ISS to obtain lifetime values, Figure 11 shows a TCSPC data set taken for 20 μM DOX@DODAB:MO labelled with the 9AS probe, the fitted multiexponential curve, as well as the IRF data.

4.2 Developed Matlab algorithm

A new fluorescence lifetime analysis tool was implemented using Matlab. Nonlinear least-squares solver *lsqcurvefit* was the basis of this function. It finds coefficients for given equation (Equation 9) with given input data and the observed output, where *xdata* and *ydata* are matrices or vectors, and the function is a matrix-valued or vector-valued function.
This function was mainly chosen because coefficients can have lower and upper bounds while other functions do not. Rather than compute the sum of squares, *lsqcurvefit* requires the user-defined function to compute the vector-valued function. Developed algorithm is available in appendix A.

The fit function gave very good results that were compatible with those acquired with Vinci Analysis by ISS. The example of fit can be seen in Figure 12. The results from both methods are discussed below.

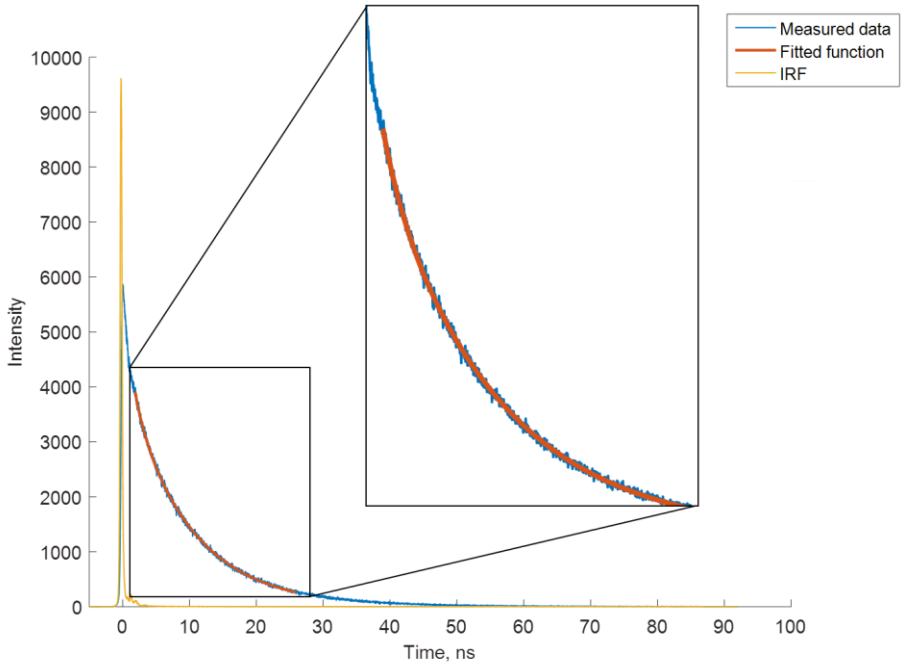

Figure 12. *TCSPC curve of the 9-AS probe inserted into a 20μm DOX@DODAB:MO liposome at 40 C shown together with the measured instrument response function (IRF) and the fit function using a two exponential fit model and the developed Matlab algorithm for analysis.*

For DODAB:MO liposomal formulations with varying DOX concentrations, the fluorescence decay measurements show steeper decay curves for higher DOX concentrations. The fit accuracy allows identifying these fluorescence lifetime differences, which indicate that a lifetime quenching process occurs (Figure 13).

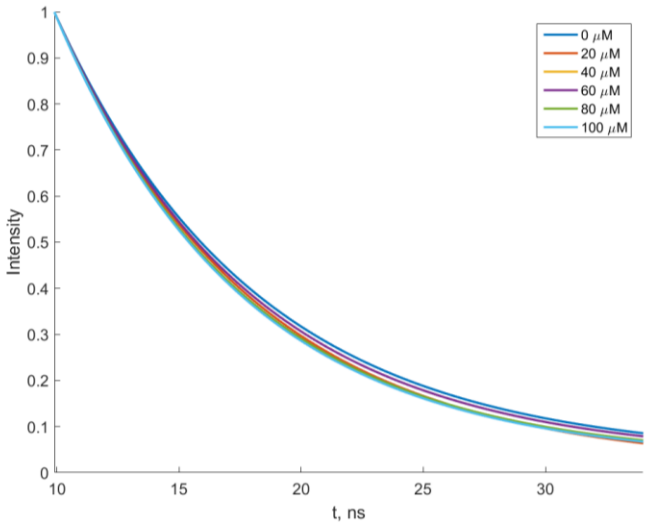

Figure 13. *DOX concentration-dependent fitted TCSPC data taken on 9-AS probes inserted into DODAB:MO liposomal formulations (developed Matlab algorithm was used)*

4.3 Comparison of available fitting methods

As discussed above, two data processing methods were tested - commercial software ISS Vinci and Matlab code developed in this thesis. Figure 14 (A-D) show the mean fluorescence lifetime results determined for the same data sets with the different fit algorithms (all values are also given in Appendix B). The fluorescence lifetimes of the n-AS probes in DODAB:MO at various DOX concentrations determined using the Vinci software vary between 7.60 – 10.69 ns, while the fit with Matlab leads to lower values ranging between x and 6.90 - 8.74 ns.

Haldar et al. report $<\tau>$ values of 5.72, 8.14, 10.64, 10.88 ns for 2-AS, 6-AS, 9-AS and 12-AS probes respectively in 1,2-Dioleoyl-sn-glycero-3-phosphocholine (DOPC) membranes (Haldar et al. 2012). The differences found between the obtained experimental values and the values reported could be explained by different chemical composition of DODAB:MO (1:2) and DOPC membranes.

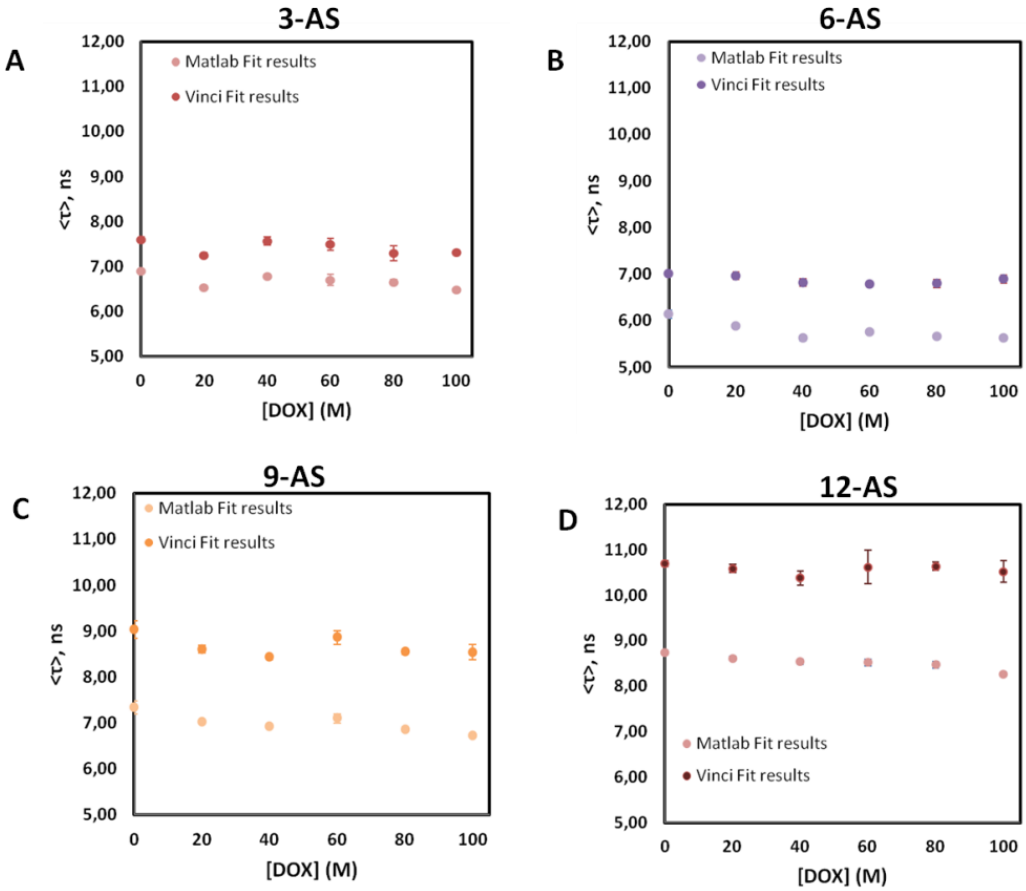

Figure 14. *Comparison of fluorescence lifetime fit results for DOX concentration-dependent data series taken on the different n-AS probes labelling the DODAB:MO liposomal formulations. ISS Vinci software and Matlab analysis algorithm were used and standard deviations are indicated. Data are shown for A: 3-AS; B: 6-AS;C: 9-AS and D:12-AS labelled liposomes, respectively.*

Absolute values obtained with the two techniques are slightly different and differ maximally by 2 ns, while the deviation in all cases is to shorter lifetimes in case of the Matlab implemented algorithm. Values calculated with Matlab code are constantly smaller than those from ISS, but as it can be seen in Figure 14 A-D standard deviations were extremely small for lifetime values acquired with Matlab. χ^2 values are reported in Appendix B and do not deviate from 1 more than 5%. For further analysis lifetime values acquired with Matlab was used.

5. RESULTS

5.1 Liposomal characterization

DLS and ELS were used to determine the size and surface charge of DODAB:MO (1:2) liposomal formulations.

5.1.1 Liposome size

The size and PdI of the DODAB:MO (1:2) liposomes without DOX were measured immediately after their extrusion. The mean size for the sample plus the standard deviation and PdI are shown in Table 3.

Table 3. *The z-average diameters (nm), polydispersity index values and zeta potential mean values (mV) obtained from measurements of DODAB:MO (1:2) liposomes*

	z-Average Diameter (nm)	**Polydispersity Index (PdI)**	**Zeta Potential Mean Values (mV)**
DODAB:MO (1:2)	118.9 ± 0.5	0.161 ± 0.01	+50.4 ± 9.5

The particle size distribution shows one single peak that corresponds to only one size population (Figure 15).

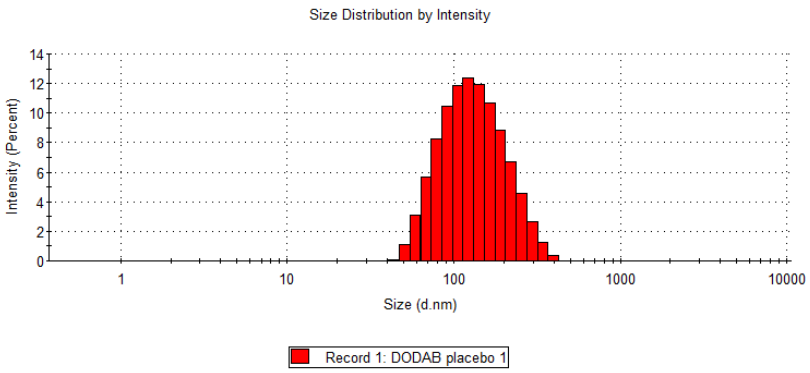

Figure 15. *DLS-obtained size distribution of DODAB:MO (1:2) liposomes in water*

A small particle size of ~100 nm was desired. The average diameter measured is 118.9 nm. The liposomes have an average PdI of 0.161. According to Malvern Instruments

user manual (2013), if the PdI is below 0.2, it can be concluded that the liposomes in the suspension have a monodisperse size distribution.

5.1.2 Liposome zeta potential

The mean ζ-potential for each sample plus the standard deviation is shown in Table 3. DODAB:MO (1:2) liposomes hydrated with only ultrapure water have a mean ζ-potential of +50.4 mV at a mean pH value ± standard deviation of 5.5±0.3, which is consistent with other reported values for the same type of liposomes (Almeida 2009). It means that produced liposomes can be considered stable as their ζ-potential is larger than +30 mV. This positive surface charge is advantageous both in terms of shelf stability, providing repulsion between the liposomes, and in terms of membrane cell adhesion as the positive charges will have higher propensity to interact with slightly negatively charged cellular membranes.

5.1.3 Nanoscale localization of the drug

Measured fluorescence emission and absorption as well as lifetime data were processed and analysed in contemplation of gaining knowledge about nanoscale localization of DOX in DODAB:MO (1:2) liposome.

5.1.3.1 Spectroscopic analysis of n-AS probes inserted into DODAB:MO(1:2) liposomes loaded with various concentrations of DOX

Fluorescence emission spectra were measured for 3 AS, 6 AS, 9 AS and 12 AS labelled DODAB:MO(1:2) samples with varying concentrations of DOX 0, 20, 40, 60, 80 and 100 μM. Excitation wavelength was 379 nm. The data was processed as described in Appendix C.

The typical emission spectra of fluorescence quenching DODAB:MO (1:2) liposomes with different quencher concentrations are shown in Figure 16 A-D for the 3-AS, 6-AS, 9-AS and 12-AS probes, respectively, where it is possible to observe that the drug was able to decrease the fluorescence intensity of the fluorescence probe. Furthermore the maxima of the longer wavelength absorption band and fluorescence maxima of the fluorophore do not change in the presence of quencher. These factors ruled out the possibility of dynamic or collisional quenching process, however only the lifetime analysis can definitely confirm the quenching process.

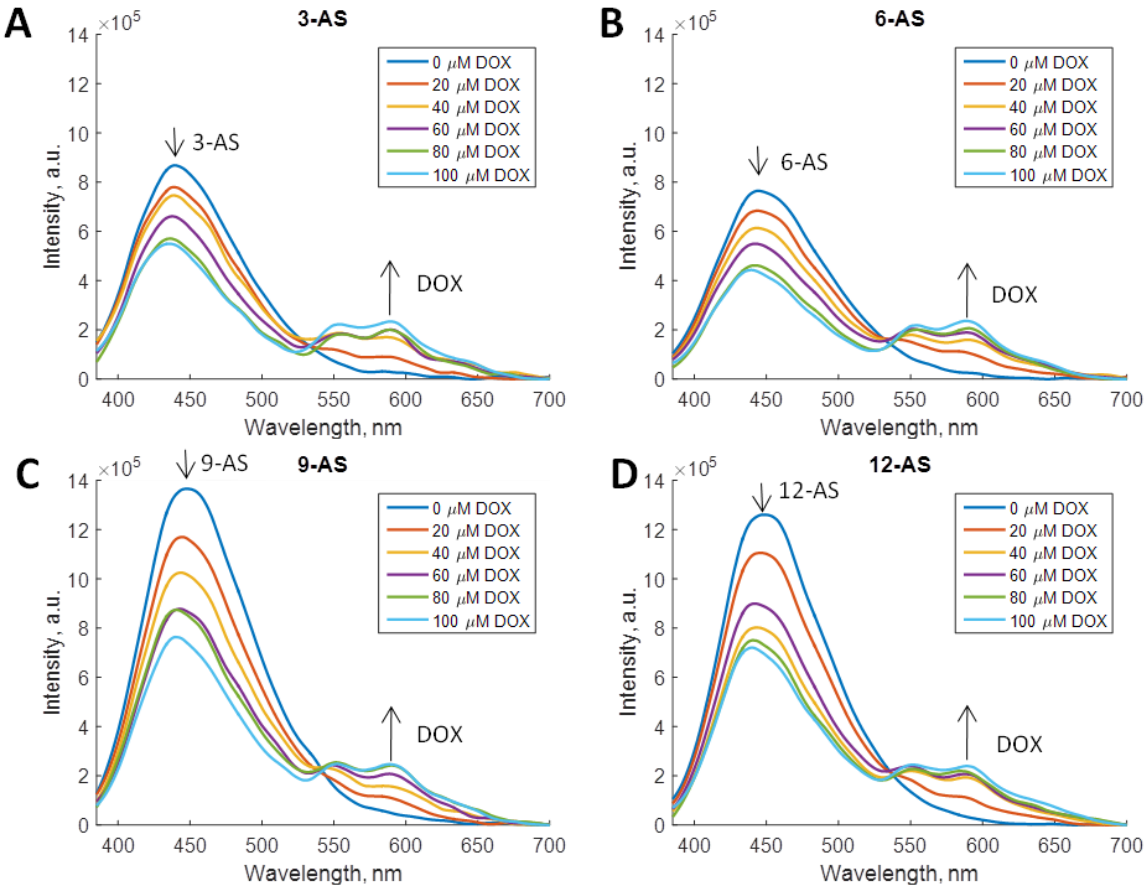

Figure 16. *Steady state fluorescence emission spectra taken from 3-AS-, 6-AS-, 9-AS- and 12-AS- labelled DODAB:MO liposomes containing varying DOX concentrations. Besides the emission peak of the n-AS labels peaking around 450 nm, also DOX emission with two bands at 650 and 580 nm is observed. Excitation wavelength was 379 nm.*

In addition, absorption spectra of all samples were recorded for all samples and used for correction of the inner filter effect due to absorbance of the light when the samples are excited. The absorbance spectra are shown in Figure 17 (A to D) for the 3-AS, 6-AS, 9-AS and 12-AS probes respectively. The peak absorbance values for each sample at 385 nm are used to correct the inner filter effect using Equation (1) and (2), and values are given in Appendix D. The absorbance seemingly rises as the concentration of DOX increases. The distances between absorbance spectra of *n*-AS labelled DODAB:MO(1:2) containing varying concentrations of DOX are equal, with exception of two curves (6-AS labelled DODAB:MO(1:2) with 100 μM DOX and 12-AS labelled DODAB:MO(1:2) with 40 μM DOX). The differences might have arisen due to pipetting error.

As the drug partitions inside the liposomes, the effective concentration $[Q]_m$, (determined using Equation 4) was used to determine the Stern-Volmer constant and therefore $[DOX]_m$ values are also used in the Stern-Volmer plots.

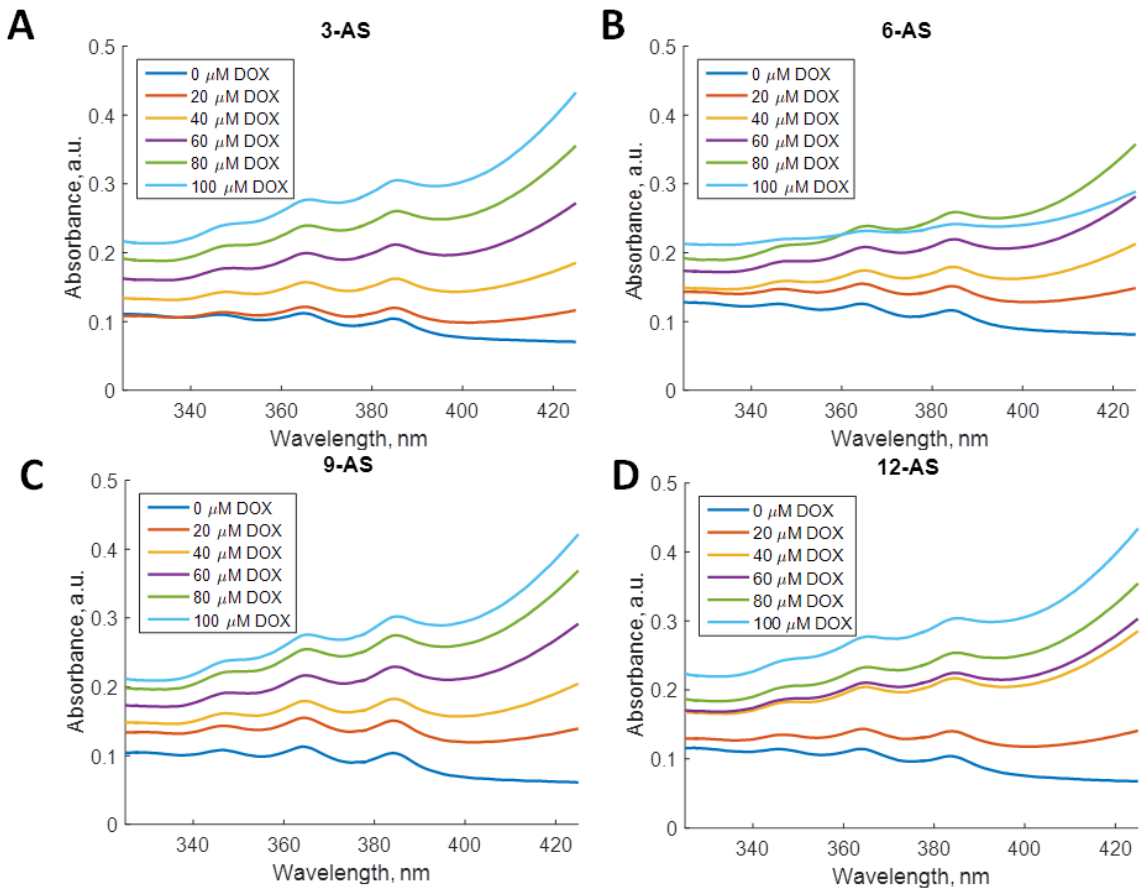

Figure 17. *Absorbance spectra taken from 3, 6, 9 and 12-AS labelled DODAB:MO (1:2) liposomes containing varying DOX concentrations shown in A,B, C and D, respectively. For correcting the inner filter effect the peak at around 385 nm was analysed.*

The plots in Figure 18 show the steady-state Stern-Volmer plots for the fluorescence emission uncorrected (dashed line) and corrected for the inner filter effect (bold line) for all the samples of DODAB-MO (1:2) labelled liposomes with increasing DOX concentrations. For the various *n*-AS probes the Stern-Volmer plots present linear behaviour with significantly different slopes indicating different quenching efficiencies of the probes by the quencher (DOX). It is also visible that neglecting absorption correction of the inner filter effect here leads to smaller Stern-Volmer constants.

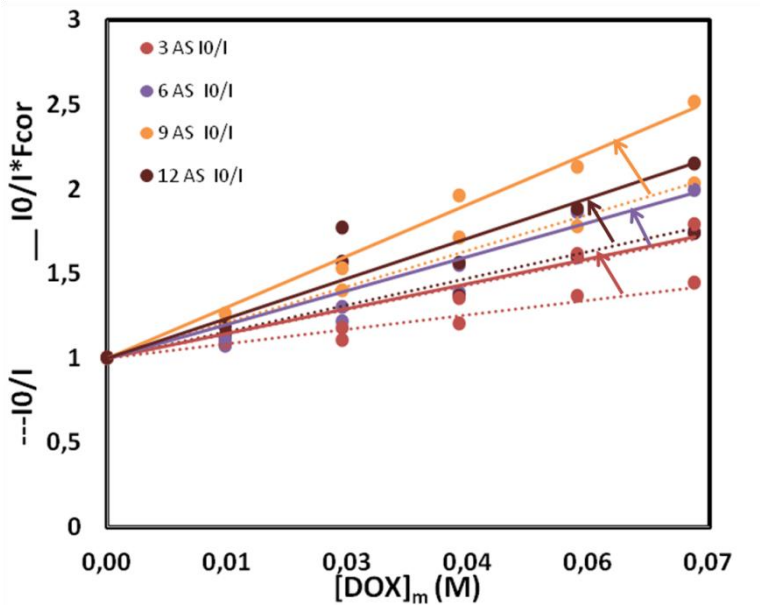

Figure 18. *Steady-state Stern Volmer plots. Relative fluorescence intensity changes (Io/I) measured at the fluorescence peak maximum located at 485 nm (---) and as corrected for inner filter effect using the steady state absorption data (___) for 3, 6, 9, and 12-AS labelled DODAB:MO (1:2) liposomes in dependence of encapsulated anti-cancer drug DOX. The concentration of DOX is given as the effective drug concentration inside the DODAB:MO(1:2) lipid membrane, considering the known partition coefficient of DOX in DODAB:MO.*

Figure 20 shows the dynamic Stern-Volmer constant differences for the different AS probes - small decrease of the fluorescence lifetimes in presence of DOX is observed for 3-AS, 6-AS, 9-AS and 12-AS labelled DODAB:MO(1:2). Steepest slope for the relative fluorescence lifetime, thus highest quenching, was observed for the 6-AS probe.

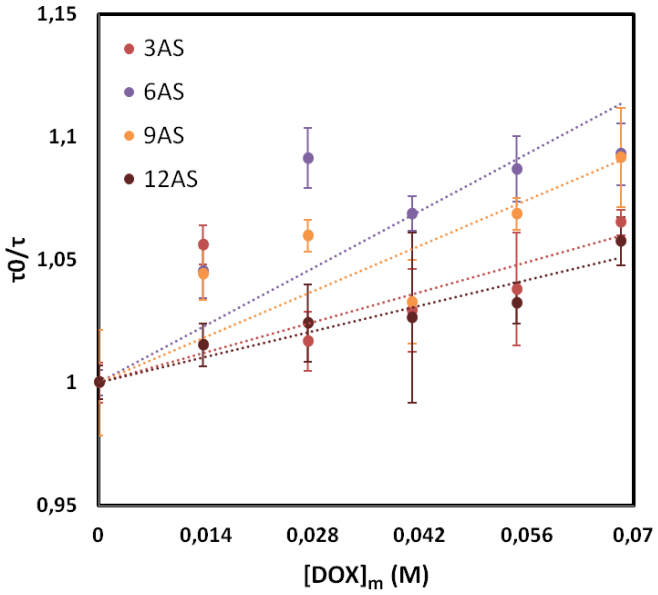

Figure 19. *Dynamic Stern-Volmer plots. Relative average lifetime changes for all n-AS probes inserted into DODAB:MO(1:2) liposomes of varying concentrations of encapsulated DOX.*

5.1.3.2 Determination of Stern-Volmer constants

To determine K_{SV}, the membrane effective concentration of the quencher in the lipid membrane $[Q]_m$ was calculated using Equation (4). Stern-Volmer constants were obtained from the corrected relative fluorescence steady state emission values $I_0/I*F_{corr}$ plotted as a function of $[Q]_m$ and Stern-Volmer constant was determined from the slope of the linear fit (Figure 20). The dynamic constant K_D was determined from linear fits of drug concentration dependent fluorescence lifetime results (Figure 19, 20).

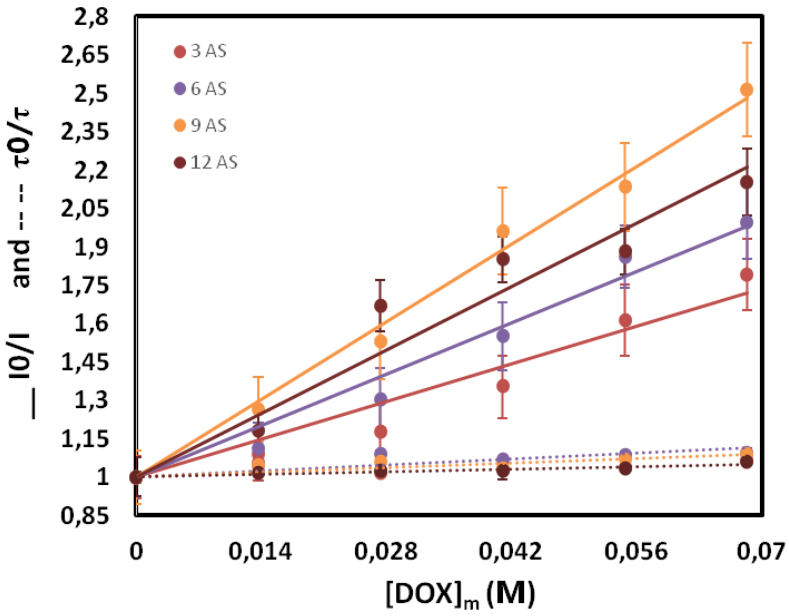

Figure 20. *Combined inner filter corrected steady state and dynamic Stern-Volmer plot used to determine the Stern-Volmer constant K_{SV}, the static K_S and dynamic K_D quenching constant. The concentration of DOX is given as the effective drug concentration inside the DODAB:MO(1:2) lipid membrane, considering the known partition coefficient of DOX in DODAB:MO. The TCSPC data was fitted using a bi-exponential model, and a weighted average of the lifetime components are used to represents the fit results.*

All results are summarized in Table 4 which presents the determined values of K_{SV}, K_s and K_D values, with $K_s = K_{SV} - K_D$.

Table 4. *Stern-Volmer constant*

DOX	K_{sv} (M^{-1})	K_D (M^{-1})	K_s (M^{-1})
3 AS	10,6 ± 3,15	0,9 ± 0,3	9,7± 3
6 AS	14,4 ± 3,19	1,7 ± 0,3	12.7 ± 3
9 AS	21,8 ± 3,35	1,3 ± 0,3	20,5 ± 3
12 AS	17,8 ± 2,59	0,7 ± 0,3	17,1 ± 2,5

The bimolecular quenching constant K_q leads to better comparability in case the reporter dyes have different fluorescence lifetimes in absence of a quencher. As this is the case

for the different *n*-AS probes it is beneficial to analyse the bimolecular quenching constants (K_q):

$$K_q = \frac{K_{SV}}{\tau_0} \ , \tag{14}$$

where τ_0 is the fluorescence lifetime of the *n*-AS probe in DODAB:MO (1:2) liposomes that was experimentally measured in the absence of quencher.

The determined Stern-Volmer constants K_{sv}, measured fluorescence lifetime of *n*-AS probes in DODAB:MO liposomes and in absence of the quencher τ_0 and from these values derived bimolecular quenching constants K_q are summarized in Table 5. 9-AS probe showed the highest K_q value followed by 12-AS, 6-AS and 3-AS probes.

Table 5. *Stern-Volmer and bimolecular quenching constants of n-AS probes*

Probe	K_{sv}, M^{-1}	τ_0, ns	K_q, $M^{-1}s^{-1}$
3 AS	10,6	6,90	1,54 *10^9
6 AS	14,4	6,14	2,35 *10^9
9 AS	21,8	7,33	2,97 *10^9
12 AS	17,8	8,74	2,04 *10^9

K_q assesses the quenching and indicates the accessibility of the fluorophores to the quencher (Lakowicz 2006a). Therefore, the analysis of the K_q values (Table 5) indicates that 9-AS is the most efficient quencher of the DOX followed by 6- and 12-AS. Diffusion-controlled quenching in homogeneous solvents typically results in values of $K_q \sim 1*10^{10} M^{-1}s^{-1}$ (Lakowicz 2006a). The smaller K_q values around 1,5 *10^9 to 3 *10^9 are in agreement with the reported values found for fluorophores bound to macromolecules (Lakowicz 2006a) and can result from the fact of the fluorophore being immobilised in the lipid membranes.

5.1.4 Förster Resonance Energy Transfer (FRET) analysis

FRET analysis was based on measured steady state fluorescence emission data, where one can see that with increased concentration of DOX in *n*-AS labelled DODAB:MO(1:2) system, the intensity of *n*-AS peak (around 440 nm) decreases (Figure 16 A-D), and simultaneously the peak intensity of a DOX emission peak around 600 nm increases with increased DOX concentration. Thus, the hypothesis can be stated that the system contains FRET donor-acceptor pair where *n*-AS probe acts as donor and DOX as acceptor. Figure 21 shows relative changes of fluorescence emission peaks at 440 nm and 600 nm as function of acceptor (DOX) concentration for each *n*-AS probe. The highest relative decrease in intensity values at 440 nm (donor) peak (Figure 21 dashed lines) is observed for the 9-AS labelled DODAB:MO system, followed by 12-AS, 6-AS

and finally 3-AS systems. An interesting trend appears when acceptor (DOX) peak of the system at 600 nm is analysed. The intensity at this peak increases as DOX concentration is increased. The relative changes (Figure 21 bold lines) I_a/I_d show that the least increase in acceptor peak is for 9-AS labelled DODAB:MO system followed by 12-AS, 6-AS and finally 3-AS. Thus, even though the system with 9-AS probe has the strongest decrease of emission intensity at the donor peak, it also is the system with least increase of emission intensity at the acceptor peak.

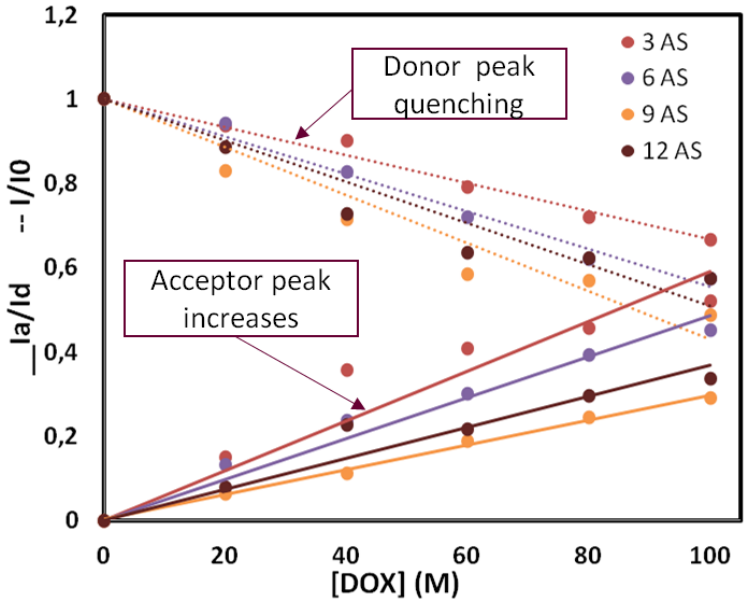

Figure 21. *FRET observation between n-AS donor and DOX acceptor molecules in DOX concentration-dependent fluorescence emission spectra taken from DODAB:MO liposomal formulations. The relative changes of the fluorescence emission peak at 440 nm, associated with the n-AS emission (I/I0) (donor peak quenching) and the relative change of intensity of the acceptor peak at 600 nm Ia divided by the intensity Id of the n-AS probe at the considered DOX concentration (acceptor peak rise) are shown for the different n- AS probes.*

For the calculation of the distance between donor (D) and acceptor (A) molecules Equation 10 was used. Transfer efficiency E was calculated using the relative fluorescence intensity (Equation 12).

In order to calculate the D–A distance it is necessary to know R_0 (Equation 13), which in turn depends upon κ^2, n, Q_D, and $J(\lambda)$. These values must be known to calculate the distance. The refractive index (n) is 1.35 and a random orientation between D and A is assumed which leads to $k^2=2/3$.

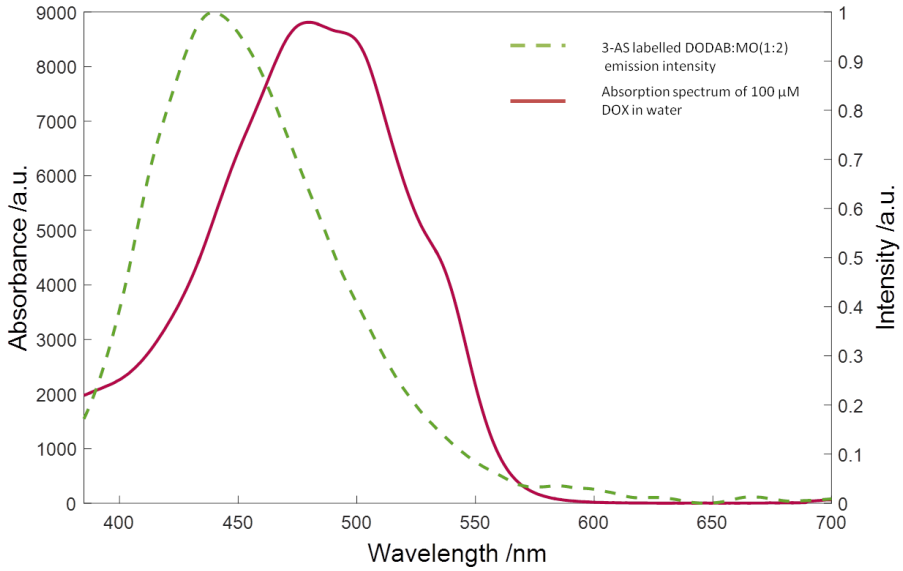

Figure 22. *The overlap of the 3-AS labelled DODAB:MO(1:2) emission spectrum with the absorption spectrum of the 100 μM DOX in water.*

The overlap integral J(λ) was evaluated for each *n*-AS – DOX (D–A) pair. The larger the overlap of the emission spectrum of the donor with the absorption spectrum of the acceptor, the higher is the value of R_0. J(λ) was evaluated using a|e - UV-Vis-IR Spectral Software from Fluortools.com. First, the acceptor molar absorption spectra was recalculated using the extinction coefficient ε. Extinction coefficient for DOX ε_{Dox}=10410 $M^{-1}cm^{-1}$ at λ=481nm was obtained from literature (Tian et al. 2003). Then DOX absorption value at peak (λ=481nm) A_{481} was selected from the measured data and multiplication coefficient was calculated to obtain the desired extinction coefficient spectrum:

$$a = \frac{\varepsilon_{Dox}}{A_{481}} = \frac{10410}{0.8810} = 11818.8\, M^{-1}cm^{-1} \qquad (14)$$

When DOX absorption extinction coefficient spectrum is in units of $M^{-1}cm^{-1}$ the spectral overlap integrals between acceptor absorption and donor emission spectra can be calculated. DOX absorption extinction coefficient spectrum and 3-AS, 6-AS, 9-AS and 12-AS emission spectra were plotted in the a|e graph window and spectral overlap integral was calculated (see Figure 22).

Quantum yield values for the *n*-AS donor probes (Q_D) have been reported as inserted into a variety of systems, for example, in sonicated dispersions of dipalmitoyl phosphatidyleholine (Thulborn et al. 1979), in cytosol haemoglobin (Eisinger & Flores 1982), in Triton X-100 micelles and in sodium dodecyl sulphate (SDS) micelles (Berberan-Santos & Prieto 1987) summarized in (Table 6). The quantum yield values in sonicated dispersions of dipalmitoyl phosphatidyleholine, in cytosol haemoglobin and in Triton X-100 micelles are similar, whereas values in SDS micelles differ.

Since Q_D is used as the sixth root in the calculation of R_0, small errors in Q_D do not have a large effect on R_0, the quantum yields obtained in the chemically most comparable environment for the n-AS probes therefor shall be selected for the further FRET analysis.

Table 6. *Quantum yield values of the donors (n-AS probes) in different systems*

Probe	**In sonicated dispersions of dipalmitoyl phosphatidyleholine** (Thulborn et al. 1979)	**In cytosol hemoglobin** (Eisinger & Flores 1982)	**In Triton X-100 micelles** (Berberan-Santos & Prieto 1987)	**In SDS micelles** (Berberan-Santos & Prieto 1987)
2 AS	0.35	0.33	0.14	0.07
3AS	-	-	0.18	0.07
6 AS	0.41	0.4	0.31	0.08
9 AS	0.4	0.44	0.41	0.12
12 AS	0.47	0.47	0.55	0.15

Figure 23 shows the chemical structures of the studied *n*-AS molecular environments. One can see that dipalmitoyl phosphatidyleholine molecule (Figure 23 D) has two carbon chains and a headgroup. This structure is the most similar to DODAB's, therefore quantum yield values in sonicated dispersions of dipalmitoyl phosphatidyleholine micelles were used for the calculation of the D-A distance.

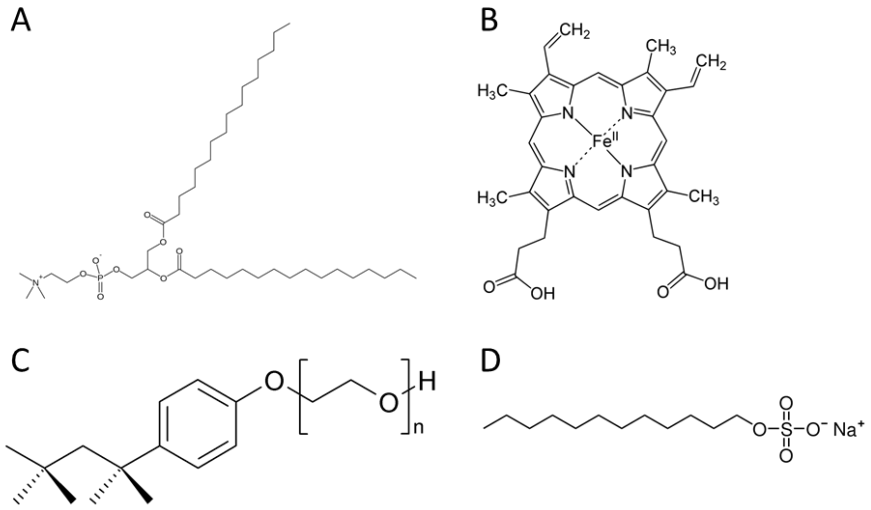

Figure 23. *Chemical structures of systems used elsewhere in combination with n-AS probes. A: dipalmitoyl phosphatidyleholine (Wikimedia 2007b); B: haemoglobin (Wikimedia 2016); C: Triton X-100 (Wikimedia 2007a); D: SDS (Wikimedia 2008)*

The set of Equations 13, 14 and 15 is used for the determination of E, R_0 and subsequently for the determination of the distance $r_{D\text{-}A}$ and under consideration of the SDS lifetime values (Table 6), a measured DOX absorption spectrum (see Figure 22) and the

measured steady state fluorescence emission spectra measured in 20μM DOX@ DODAB:MO (1:2) liposomal solutions for the different probes shown in (Figure 16 A-D, orange curves). This way calculated D-A distances are displayed in Table 7, along the determined spectral overlaps J(λ) and the FRET efficiency parameter E.

The shortest distance, 24.8 Å, is between 9-AS and DOX molecules. Then 3-AS (25.2 Å) and 12-AS (25.7 Å) distances follow, the longest is between 6-AS and DOX molecules (27.7 Å).

Table 7. *Determined J(λ) and calculated E and D-A distances for n-AS and DOX FRET pair*

Probe	J(λ), $nm^4/(M*cm)$	E	r_{D-A}, Å
3AS	$2.7E^{+14}$	0.87	25.2
6 AS	$2.96E^{+14}$	0.83	27.7
9 AS	$2.93E^{+14}$	0.90	24.8
12 AS	$3.17E^{+14}$	0.90	25.7

Q_d value used obtained from sonicated dispersions of dipalmitoyl phosphatidyleholine (Thulborn et al. 1979)

5.2 *In Vitro* studies of cancer cell uptake

The cellular uptake of the liposomal formulation was evaluated using two cancer cell lines: A431 and A549. Comparison was made between DOX@DODAB:MO and free DOX and DOX@DODAB:MO and the commercial DOX formulation Doxil®.

5.2.1 Comparison of DOX@DODAB:MO versus free DOX uptake

Both cancer cell lines, A431 cells (epidermoid carcinoma) and A549 cells (lung carcinoma), were exposed to the liposomal formulation DOX@DODAB:MO (1:2) and to free DOX solutions with overall identical 5 μM DOX concentrations. The samples were fixed after 1, 2, 4 and 6 hours of exposition to the DOX containing solutions. The DOX fluorescence intensity distribution was measured in A431 and A549 cells using confocal microscopy with DOX excitation at 488nm and signal collection between 530 and 688 nm.

Images were created using Fiji and using the z-projection (sum) along z-stacks taken with a Zeiss LSM 780 confocal microscope across entire cells. A Gaussian Blur filter with radius 0.3 μm was used to even the background. Brightness and contrast was adjusted for 1 h samples and kept identical for all images that were selected for the comparison.

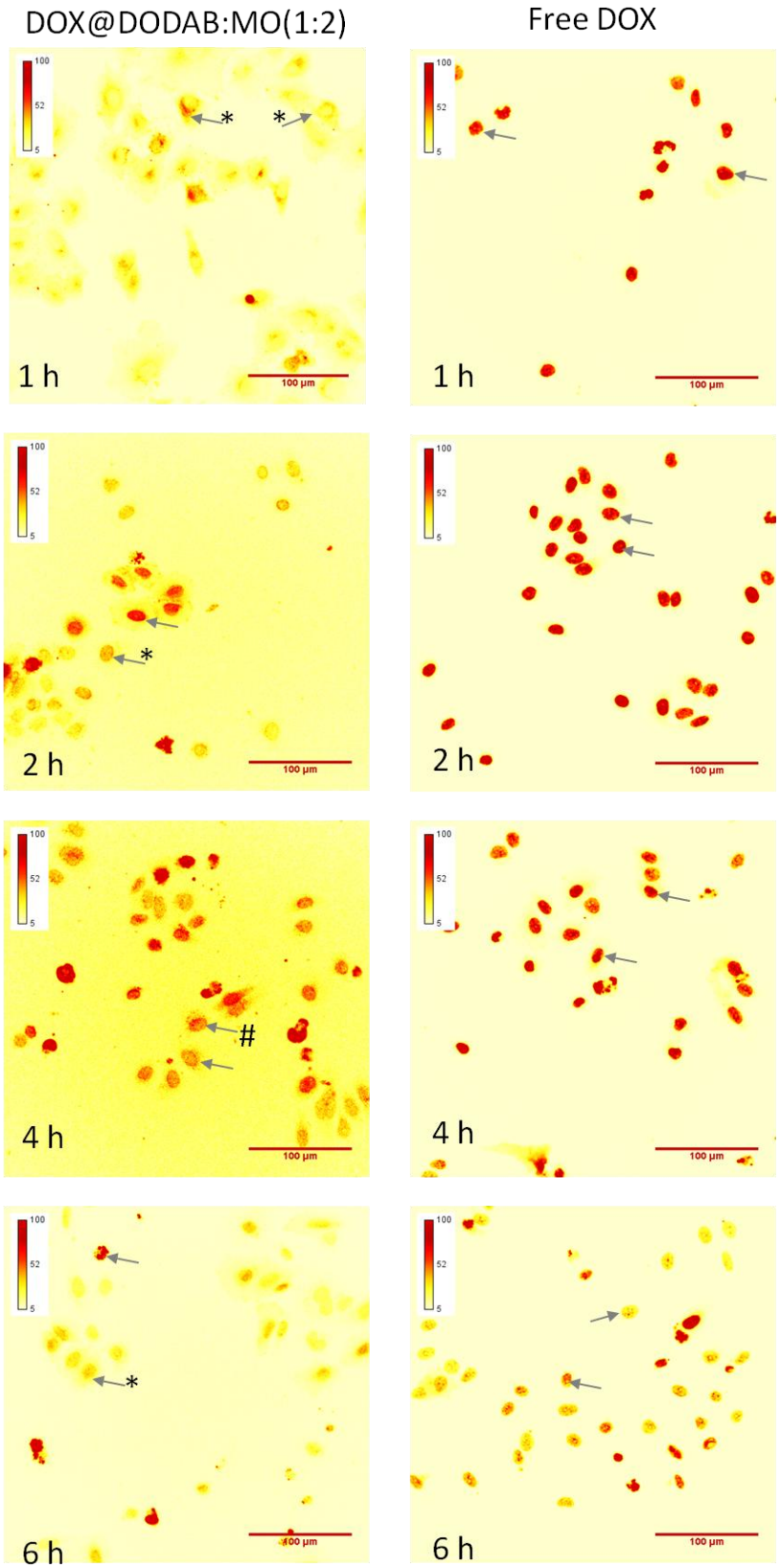

Figure 24. *DOX emission signal in confocal z-stacks projections and taken from A549 cells incubated for 1 h, 2 h, 4 h and 6 h with 5µM DOX@DODAB:MO (1:2) and 5µM free DOX solutions. Grey arrows indicate the main differences described in the text.*

Representative confocal microscopy results of A549 cells incubated with DOX@DODAB:MO (1:2) and free DOX solutions as selected from 8 measurements per fixed time point taken on two independently prepared cell samples are shown in Figures 24.

Figure 24 (left) shows that after 1 h of incubation with DOX@DODAB:MO (1:2) intensity can be observed inside the cells and high intensity in the nucleus and close around it localizing in intensity spots, indicating lysosomal accumulations (indicated with grey arrow and *). At 2 h and 4 h gradual increase of the intensity in nucleus and cytoplasm was observed, in addition some high intensity spots forming ´´clouds´´ (indicated with grey arrow and #) around the nucleus were noticed. After 6 h almost all intensity is in the nuclei, some high intensity spots remain inside the cytoplasm/lysosomes. Some cells have rounded up after longer exposure as can be seen from the transmission images (shown in Appendix D) and thus the intensity in those seems higher at chosen brightness/contrast settings.

For the interaction of free DOX solutions with A549 cells, some differences can be observed in the time dependent uptake of the drug by cells (see Figure 24 right). After 1 h of incubation with free DOX, a more homogenous DOX distribution is observed inside the cytoplasm and also intensity inside the nucleus can be observed. After 2 h the intensity in nucleus and cytoplasm increased. After 4 h almost all DOX is inside the nucleus and after 6 h of exposure to free DOX solution some cells have high intensities in the nucleus but the majority of cells have decreased overall intensity in the nuclei while only some areas of nuclei have higher intensities. This phenomenon could be due to DOX intercalation with DNA, like the one that can be observed with e.g. Hoechst 33342 nucleus stain at various cell cycle stages, when the chromosomes condensate.

5.2.1.1 Cell line A-431

Representative confocal microscopy results of A431 cells incubated with DOX@DODAB:MO (1:2) and free DOX solutions as selected from 8-10 measurements per fixed time point taken on two independently prepared cell samples are shown in Figure 25. The transmission images are shown in Appendix D.

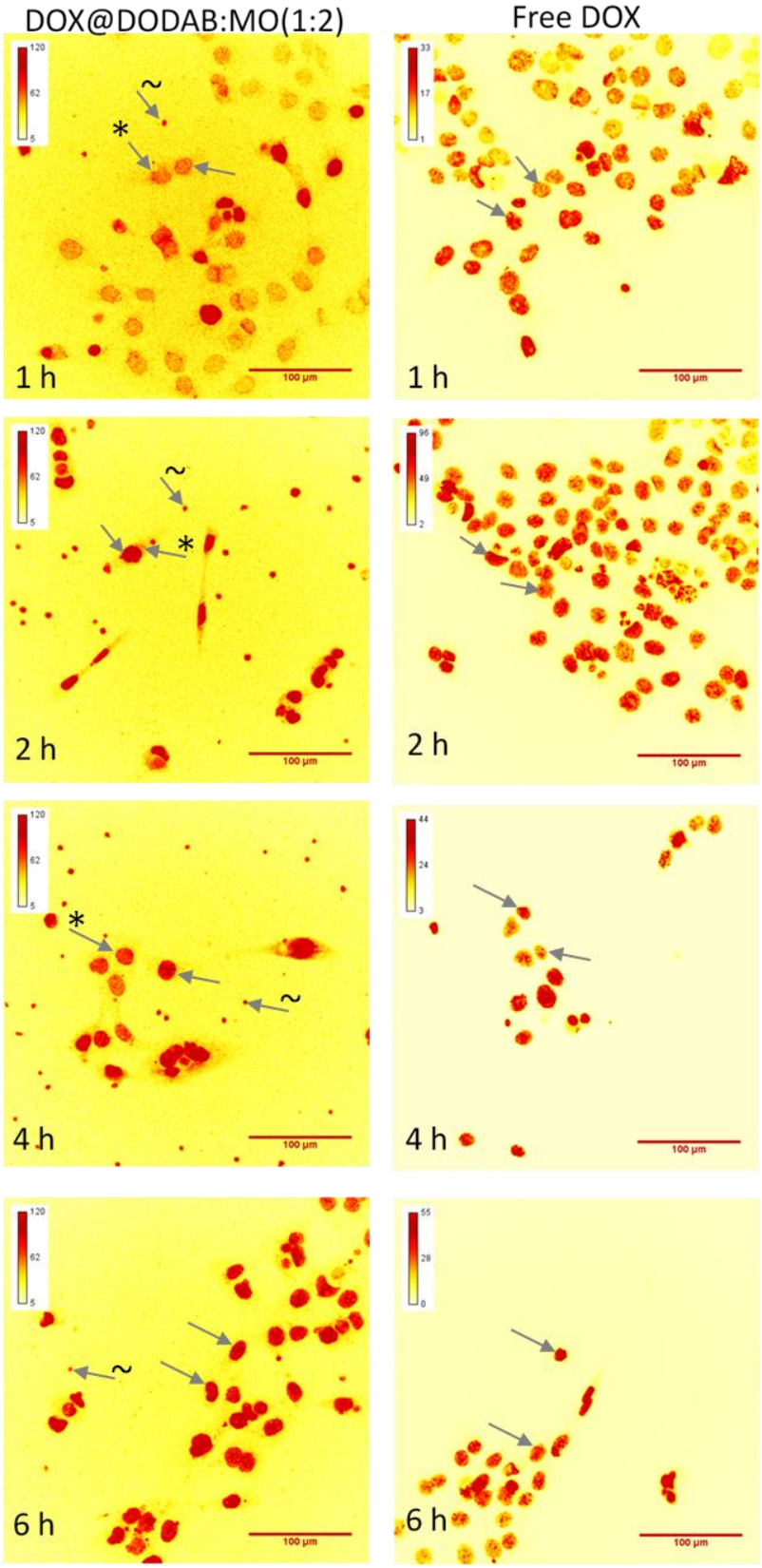

Figure 25. *DOX emission signal in confocal z-stacks projections and taken from A431 cells incubated for 1 h, 2 h, 4 h and 6 h with 5µM DOX@DODAB:MO (1:2) and 5µM free DOX solutions. Grey arrows indicate the main differences described in the text.*

A431 cells tend to grow in large groups and usually they are not forming one uniform layer but, in contrary, grow in some cases one on top of another. Because of that, some areas of the cell nuclei seem to have extremely high fluorescence intensity when the z-projection along z-stacks was performed and adjusted brightness/contrast settings were applied. A Fiji macro was developed, that automatically adjusted colour scale settings for each image (Appendix D) and used for image processing for the confocal data taken of A431 cells incubated with free DOX.

When A431 cells were incubated with DOX@DODAB:MO (Figure 25 left column) already after 1 h accumulation of DOX in the nucleus was visible, furthermore, DOX appears in intensity spots around the nucleus suggesting lysosomal colocalization (Figure 25, left column, indicated with grey arrow and *). DOX liposome uptake in this cell line occurs much faster than in the A549 cell line. After 2 h nuclei have high DOX intensity with some high intensity spots close to the nucleus. After 4 h of incubation with the liposomes nuclei have high DOX intensity and homogeneous intensity is present also in cytoplasm. After 6 h intensity in nuclei and cytoplasm has increased even more.

In addition, an interesting phenomenon was observed, when A431 cells were incubated with DOX@DODAB:MO – small intensity spots with high DOX intensities were observed outside of cells and widely distributes across the cover slip surface (indicated with grey arrow and ~). These DOX emission spots were of small size (~10 μm) and the intensities increased for samples fixed at later time points.

For samples exposed to free DOX (Figure 25, right column), homogeneous intensity inside the nucleus after 1 h was observed also there was presence of DOX in cytoplasm. After 2 h exposure to free DOX almost all DOX intensity is in nuclei, observed overlapping of the cells that might lead to higher intensity regions. After incubation of the cells with free DOX for 4 h and 6 h, DOX intensity has increased over time, almost no intensity is observed in the cytoplasm.

5.2.2 Comparison of DOX@DODAB:MO versus Doxil® uptake

Both cancer cell lines, A431 cells (epidermoid carcinoma) and A549 cells (lung carcinoma), were exposed to the liposomal formulation DOX@DODAB:MO (1:2) and to commercial DOX - Doxil® - solutions with overall comparable 40 μM DOX concentrations. The samples were fixed after 1, 2, 4 and 6 hours of exposition to the DOX containing liposomal solutions and DOX fluorescence intensity in confocal images was measured.

Images were created using Fiji and using the z-projection along z-stacks taken with a Zeiss LSM 780 confocal microscope across entire cells. A Gaussian Blur filter with radius 0.3 μm was used to even the background. Brightness and contrast was adjusted for 1 h samples and kept identical for all images that were selected for the comparison.

5.2.2.1 Cell line A-549

Representative confocal microscopy results of A549 cells incubated with DOX@DODAB:MO (1:2) and Doxil® solutions and as selected from 8-10 measurements per fixed time point taken on two independently prepared cell samples are shown in Figure 26.

Figure 26 (left column) shows A549 cells exposed to DOX@DODAB:MO (1:2) liposomal solutions. After 1 h high intensity in the nucleus can be observed and close around it DOX appears in intensity spots (indicated with grey arrow and *), in addition there is DOX intensity in cytoplasm. At 2 h and 4 h gradual increase of the intensity in nucleus and cytoplasm was observed. After 6 h almost all intensity is in nucleus and it is very high, some intensity spots remain inside the cytoplasm. The background intensity is low. Some cells have rounded up and some have distorted shapes after longer exposure and thus the intensity in those seems higher at chosen brightness/contrast settings. The transmission images are shown in Appendix D.

Figure 26 (right column) shows A549 cells exposed to Doxil® solutions. After 1 h of incubation with Doxil® more DOX distribution inside the cytoplasm and nucleus can be observed. The intensity in cytoplasm is rather homogeneous and only few localized intensity spots around the nucleus are observed, which is distinct in the sample with DOX@DODAB:MO (1:2) (indicated with grey arrow and *). The homogenous intensity may indicate a drug diffusion process through the cell membrane rather than an endocytosis uptake suggested for the liposomal uptake. After 2 h the intensity in nucleus and cytoplasm increased, additionally there are some bigger high intensity spots near nuclei. After 4 h DOX is inside the nuclei and in cytoplasm. Some of the nuclei have reached high intensities and at given settings reached saturation. At 6 h time point all cells have high intensities in nucleus and saturation is observed. In addition, the intensities in cytoplasm and background have increased. The background intensity is higher for samples with Doxil® than with DOX@DODAB:MO. Some cells have rounded up as can be seen in transmission images (Appendix D) and some have distorted shapes after longer exposure and thus the intensity in those seems higher at chosen brightness/contrast settings. In addition, at 6 h cell debris can be observed in form of largely scattered DOX intensity spots that are visible as spots also in transmission images (Appendix D) and could be associated to cell death (indicated with grey arrow and ~).

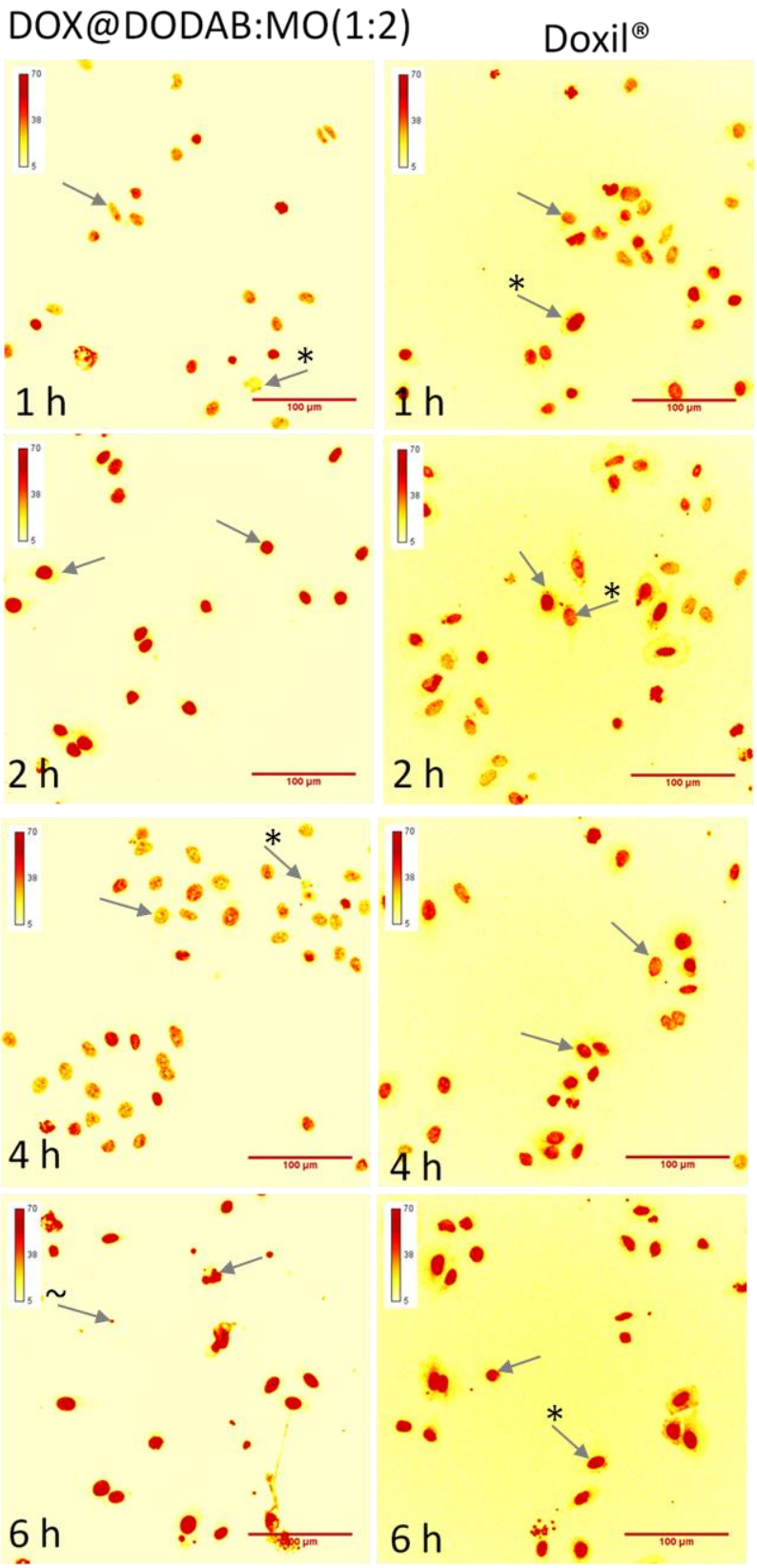

Figure 26. *DOX emission signal in confocal z-stacks projections and taken from A549 cells incubated for 1 h, 2 h, 4 h and 6 h with 40µM DOX@DODAB:MO (1:2) and 40 µM Doxil® solutions. Grey arrows indicate the main differences described in the text.*

5.2.2.2 Cell line A-431

Representative confocal microscopy results of A431 cells incubated with DOX@DODAB:MO (1:2) and Doxil® solutions and as selected from 8 to 10 measurements per fixed time point taken on two independently prepared cell samples are shown in Figure 27. The transmission images are shown in Appendix D.

As observed in previous experiments with DOX@DODAB:MO (1:2) and free DOX, also in experiments with 40 μM DOX@DODAB:MO (1:2) and Doxil® A431 cells grew in large groups and were growing sometimes one on top of another. Because of that some areas of the cell nuclei seemed to have extremely high fluorescence intensity when the z-projection along z-stacks was performed and adjusted brightness/contrast settings were applied.

In Figure 27 (left column) confocal images of A431 cells incubated with DOX@DODAB:MO are shown. After 1 h of incubation with DOX@DODAB:MO (1:2) some intensity spots indicating lysosomal accumulation of DOX (indicated with grey arrow and *), furthermore, DOX was present in the nucleus. DOX uptake in this cell line is very fast. After 2 h nuclei have increased DOX intensity with some high intensity spots in the nucleus. After 4 h, nuclei have high DOX intensity and homogeneous intensity is present also in cytoplasm. After 6 h intensity in nuclei and cytoplasm has increased even more. Once again, small aggregates across the coverslip and outside the cell areas were observed for A431 cells incubated with DOX@DODAB:MO. These aggregates were small size (~10 μm) and the intensities increased over time. Less of these spots are observed in the cell samples exposed to Doxil® liposomes only few of these intensity spots are visible in the 1h incubation image (Figure 27, right column).

For samples exposed to Doxil® high intensity inside the nucleus after 1 h was observed (Figure 27, right column), also there was presence of DOX in cytoplasm and some high intensity spots around nucleus. Overlapping of the cells might lead to higher intensity regions. After 2 h exposure to Doxil® almost all DOX intensity is in nuclei. After 4 and 6 h of incubation with Doxil®, DOX intensity has increased over time both in nuclei and in cytoplasm.

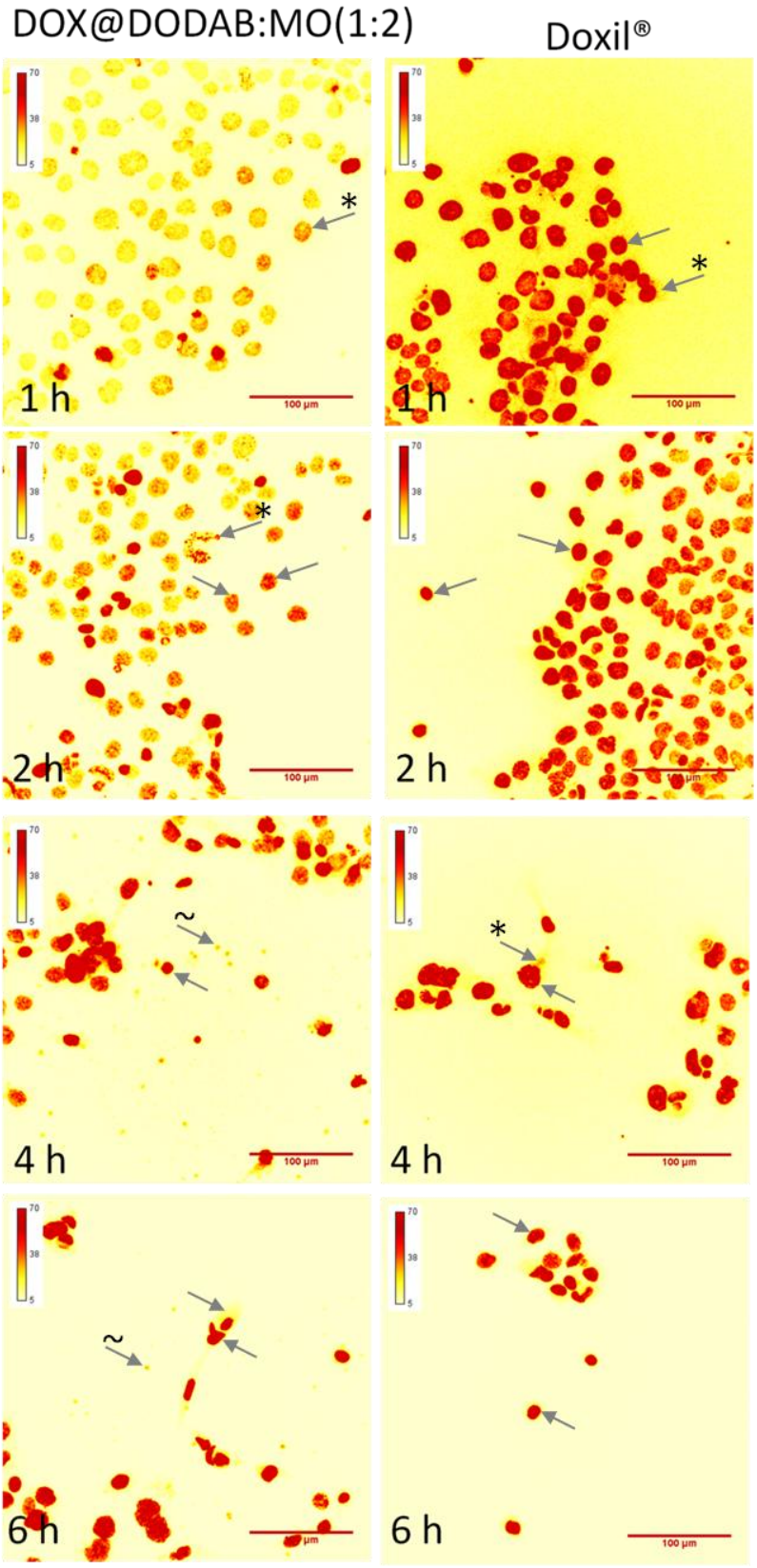

Figure 27. *DOX emission signal in confocal z-stacks projections and taken from A431 cells incubated for 1 h, 2 h, 4 h and 6 h with 40µM DOX@DODAB:MO (1:2) and 40 µM Doxil® solutions. Grey arrows indicate the main differences described in the text.*

5.2.3 Live cell studies on A431 live cells

In experiments with fixed A431 cells, DOX accumulation in nuclei was observed already after 1 h of incubation. This caused curiosity to perform live A431 cell imaging and follow the cell uptake process with improved time resolution. Live A431 cells were incubated with 40 μM DOX@DODAB:MO and the nucleus was stained with Hoechst 33342. Cells were imaged every 10 minutes and two colour z-stacks and transmission images were recorded simultaneously, starting from 30 min after exposure of the cells to the 40 μM DOX@DODAB:MO liposomal solution until 2 hours passed and cell death was observed (Figure 28).

Images were processed using freeware Fiji. Figure 28 shows the z-projections along z-stacks taken with a Zeiss LSM 780 confocal microscope across entire cells and transmission image in focus. After 30 minutes DOX intensity was high around the nucleus and there seemed to be some intensity in nucleus. After 120 minutes DOX intensity was concentrated inside of the nucleus and the round shape of the cell indicates cell death.

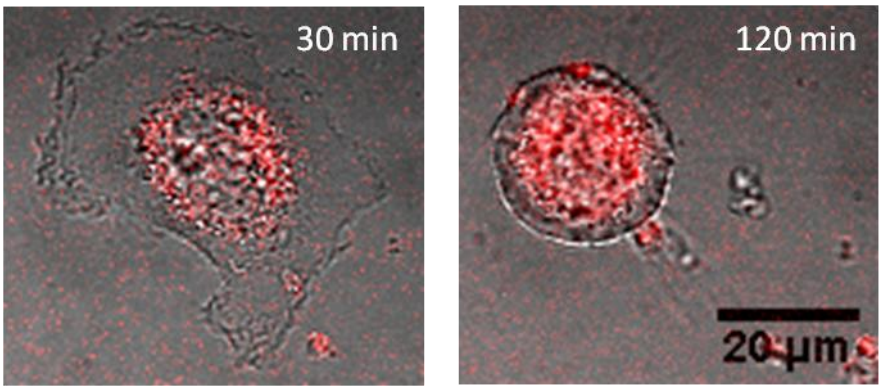

Figure 28. *Merged confocal and transmission image taken of a live A431 cell with 40 μM DOX@DODAB:MO at time points 30 and 120 minutes after addition of DOX containing suspension. Grey: in-focus transmission images, red: DOX intensity z-projections along confocal z-stacks*

The acquired 3D video of a single cell allows following the liposomal uptake process in 3D, with displayed nucleus, DOX intensity and overall shape (in transmission) seeing Figure 29. Figure 29 shows frames from such 3D video, where blue indicates the nucleus stained with Hoechst 33342 and red corresponds to DOX intensity. At the 30 min time point DOX intensity is scattered around the nucleus and in cytoplasm. At later time points this intensity slowly increases and DOX “cloud” gets more concentrated. After 90 min. formation of magenta colour can be observed thus assumption can be made that DOX has co-localized inside the nucleus. In next 30 minutes the DOX intensity in nucleus increases.

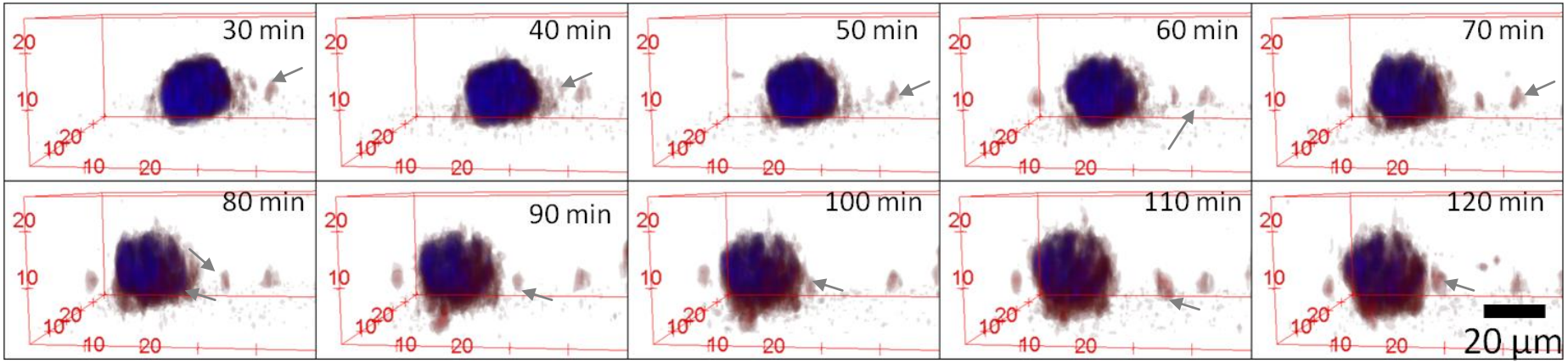

Figure 29. *Time-dependent 3D confocal two colour images, as taken from a recorded 3D video of a single A431 cell exposed to DOX@DODAB:MO(1:2) liposomes and with the nucleus labelled with Hoechst 33342 , at 10 different time points (blue: Hoechst 33342 emission, red: DOX emission). The arrows indicate the movement of recorded DOX fluorescence intensity.*

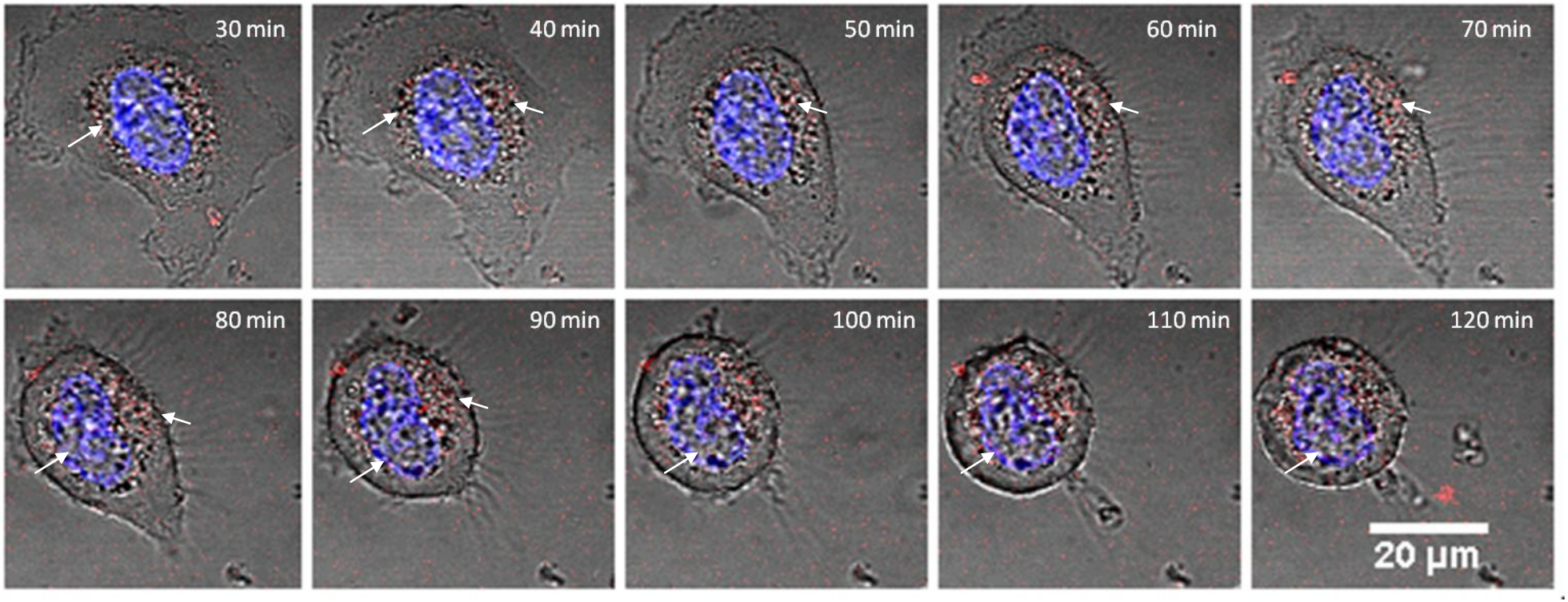

Figure 30. *Time-dependent changes of an A431 live cell exposed to DOX@DODAB:MO suspension observed in transmission and confocal imaging modes. The images show an overlay of a single center slice of a z-stack together with an in focus transmission image at 10 different time points after addition of the liposomal drug delivery system. Gray: in focus transmission images, Blue: Confocal image of the nucleus stained with Hoechst 33342, red confocal emission channel: DOX emission. The arrows indicate the movement of recorded DOX fluorescence intensity.*

Transverse slices through the cell center were taken from the 3D image data sets to verify that DOX has indeed accumulated inside the nucleus. In Figure 30 the in focus transmission image is visible in gray, blue is the nucleus stained with Hoechst 33342 and red the DOX intensity. As the intensity of DOX was not z-projected it appears much lower. Nevertheless the same trend as in the 3D video was observed. DOX intensity is clearly visible at 30 min time point around the nucleus and also in the cytoplasm. The DOX intensity distributions increase to later time points inside the overall cell and especially around and inside the nucleus.

6. DISCUSSION

6.1 Liposomal characterization

Smaller liposomes are better for intravenous drug delivery as these can reach longer circulation times. In agreement to this in the current work the main goal was to produce liposomal nanoparticles with controlled sizes preferably around 100 nm. The PdI value determined of fabricated liposomes with DLS is 0.161±0.01 and indicates that the liposomal formulation is monodisperse. Liposome size distribution of 118.9±0.5 nm was successfully achieved. High MO content in the formulation has the advantage of creating liposomal formulation with a mixture of lipid phases: DODAB forms a lamellar phase that encloses MO inverted non-lamellar phases. Based on literature review DODAB:MO (1:2) liposomal system is able to encapsulate drugs, not only at the DODAB enriched bilayer level, but also at the inverted non-lamellar MO-enriched phases at the vesicle interior (da Rocha 2014).

The surface charge of the nanoparticle is a good indicator about their shelf stability and efficiency to cross cell membranes. Liposomes with neutral charge are less stable and aggregate as there is no repulsion between the surface charge of the nanoparticles in suspension. Charged vesicles on the other hand have higher shelf stability due to the repulsion between the nanoparticles that keeps them in a stable suspension. Positively charged liposomes have the further advantage of facilitating the cellular adhesion as cell membranes are slightly negatively charged. Zeta potential of the DODAB:MO (1:2) liposomes is +50.4±9.5 mV, which means that they are stable and suited for cell adhesion.

The study of the nanoscale location of the drug in the liposome membrane plays crucial role in understanding drug-membrane interactions. For the DODAB:MO (1:2) liposomal formulation fluorescence quenching studies demonstrated to be a suited procedure. The quenching of the membrane-bound *n*-AS probes, which are characterized by the insertion of a reporter dye at different membrane depths, provide a measure of its accessibility to the quenching drug molecule. The molecular locations of the *n*-AS probe within the membrane are known and quenching studies can be used to find the location of quenchers inside the membrane. Four *n*-AS probes were used for nanoscale localization of DOX in DODAB:MO(1:2).

The Stern–Volmer plots comparing the relative intensity change I_0/I and the relative fluorescence lifetime change τ_0/τ of the reporter dyes in dependence of the effective concentration of the quencher $[Q]_m$ were studied for all *n*-AS labelled DO-

DAB:MO(1:2) liposomes encapsulating DOX at various concentrations (see Figure 21). Both, I_0/I and τ_0/τ against $[Q]_m$ curves were linear for all four *n*-AS probes. The slopes of these linear regressions correspond to the values of the Stern–Volmer constants of the quenching between the DOX and the *n*-AS probes (Table 4). The amount of dynamic quenching represented by the dynamic Stern–Volmer plot is smaller than the static quenching that is observed by steady-state fluorescence measurements at various DOX concentrations. Thus, it is concluded, that static quenching is the dominant quenching process.

The bimolecular quenching rate constants were calculated for each *n*-AS sample to remove variances due to different native fluorescence lifetimes of the reporter dyes (different τ_0). The determined K_q values are small, and indicate that the fluorophores are rather immobilised in the lipid membrane as such values resemble those observed for macromolecules, rather than dye solutions (Lakowicz 2006a). The 9-AS probe has the strongest quenching as can be seen by the relative intensity and lifetime changes as function of $[Q]_m$ and therefore biggest K_q value, followed by 12-AS, 6-AS and 3-AS. It can be concluded that DOX locates relatively close to the bilayer centre being able to interact with all *n*-AS probes.

When theoretically placing DOX and 9-AS molecules side-by-side with the polar group oriented to the polar portion of the bilayer and the aromatic portion aligned within the aliphatic tails, one can stipulate that methyl group of the DOX tetracycline ring is in proximate distance from polar 9-AS probe's part, as shown in Figure 31. This could be the reason why the fluorescence intensity of 9-AS probe is quenched the most.

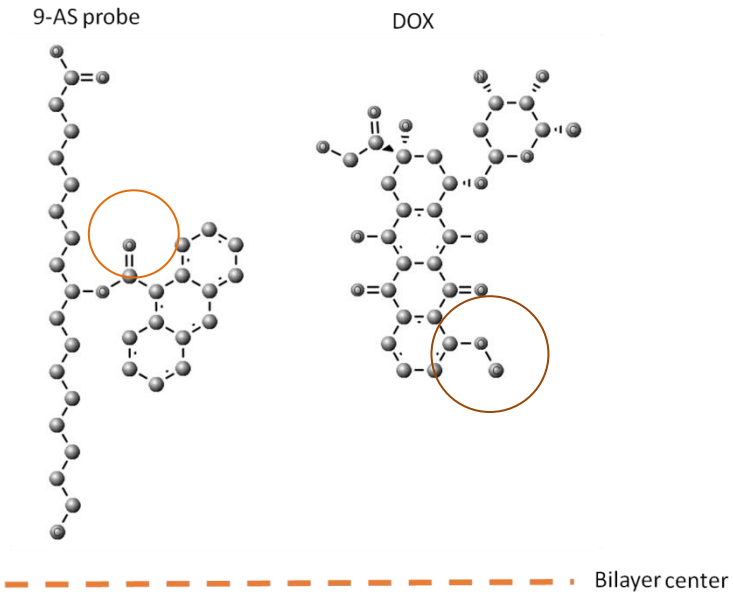

Figure 31. *Modelled DOX and 9-AS molecule orientation with respect to bilayer center. Created with software MarvinSketch 16.5.2 ©*

Another fluorescence based method particularly suited to measure the interaction of molecules in membranes is FRET. In this case, a direct transfer of energy from a fluorescent donor (*n*-AS probe) to an acceptor (DOX) occurs if their inter-molecular distance is small (typically < 10 nm). Because of small distances required between donor and acceptor FRET, possesses the clear advantage of quantifying distances well below the optical resolution limit, thus enabling measuring distances at the molecular scale. FRET analysis results are summarized in Table 7. The shortest distance determined is 24.8 Å between 9-AS and DOX molecules. Then 3-AS and 12-AS distances follow, the longest determined distance is between 6-AS and DOX molecules with 27.7 Å.

6.2 *In Vitro* studies of cancer cell uptake

The cellular uptake of a new liposomal formulation for DOX drug delivery was evaluated in two cell lines: A431 and A549. Comparison was made between the DOX@DODAB:MO liposomes and free DOX and between DOX@DODAB:MO and commercial DOX liposomal formulation Doxil®. Each fixed cell experiment was repeated twice.

Signatures of endosomal uptake are identified for both cell lines in form of intensity spots located around the nucleus for 5 μM and 40 μM DOX@DODAB:MO(1:2).

While for the A431 cells nuclear internalization of 5 μM DOX@DODAB:MO(1:2) is already visible after 1 h, the A549 predominantly show intensity spots around the nucleus at 1 h incubation time, while the nucleus is only reached at later time points, e. g. visible in the image taken after 6 h (Figure 24). Observations indicate that 5 μM DOX@DODAB:MO(1:2) leads to controlled release in time. The quicker DOX uptake in A431 cells could be due to EGF factor expression as reported in literature by Kwok & Sutherland (1991).

Small high intensity spots observed across the cover slip in A431 cell preparations at late time points for both, low and high concentration DOX@DODAB:MO(1:2), could be explained as cell debris that remained after washing of cells. The positive surface charge of DODAB:MO(1:2) and slightly negative charge of cells attract and thus create these high intensity spots.

With higher concentration of DOX in 40 μM DOX@DODAB:MO(1:2) liposomal formulations, after 1 h incubation, DOX has already reached the nucleus of A549 cells (Figure 26). Whereas, in samples incubated with 5 μM DOX@DODAB:MO(1:2) after 1 h only faint intensity of DOX can be observed (Figure 24).

Free DOX reaches the cell nucleus in both cell lines already after 1 h; after 6 h in A549 DOX signal is predominantly observed inside the nucleus (Figure 24).

Doxil® shows faster uptake than for DOX@DODAB:MO(1:2) and slower than for free DOX in both cell lines. High intensity spots around nucleus are identified for both cell lines at early time points. At 6 h the intensity in nucleus for both cell lines is high. Fluorescence intensity of DOX in A431 cells was overall higher than that in A549. This phenomenon could be due to "active loading" method used in encapsulation of DOX in Doxil® to achieve high encapsulation efficiency. In this case it is possible that high number of free DOX is available in solution transported together with the liposomes and thus diffusion of DOX into cells can occur and uptake it faster.

Live cell experiment of A431 cells taken with 10 min time resolution during 2 hours indicate that DODAB:MO(1:2) liposomal system enter the cells via the endocytosis pathway and subsequently release the DOX in controlled way (Figure 29).

7. CONCLUSIONS

The thesis work aimed to employ the opportunity to experience the international research environment in Portuguese university, University of Minho, and fully international research organization, INL. It allowed to learn different research methods from renowned professionals and to conduct wide variety of experiments independently. A huge extent of thesis was achieved due to astonishing facilities available in INL and University of Minho.

The objective of this thesis was to spectroscopically characterize pH-dependent liposome formulation and, in addition, to characterize the internalization process of DOX-loaded DODAB:MO (1:2) using advanced fluorescence imaging techniques. Successful experiments could support the potential as an anti-cancer drug delivery system of this novel liposomal formulation, as a controlled endosomal uptake of the liposomes is observed.

Different kinds of work methods were used in order to acquire the results of this thesis. After fabrication of the liposomes using the extrusion technique, cell culturing, cell fixation, and preparation for imaging and data analysis were performed. Additionally, experiments using optical spectroscopy methods using commercial devices, such as Malvern Zetasizer Nano ZS analyser, Horiba Scientific FluoroMax-4 spectrofluorometer, Perkin Elmer Lambda 950 UV-VIS-NIR spectrometer, and ChronosBH, ISS fluorescence lifetime spectrometer were used and advanced microscopy studies were performed using a Zeiss LSM 780 confocal microscope.

Based on DLS and ELS analysis the fabricated DODAB:MO (1:2) liposomal system can be considered stable and their small size suited to successfully employ EPR effect.

For nanoscale localization of the DOX within the DODAB:MO(1:2) bilayer a fluorescence quenching assay with four *n*-AS probes was used. DOX@DODAB:MO(1:2) localizes buried at deeper locations inside the lipid bilayer leading to strongest quenching at the 9-AS probe that is attached to a C atom of the lipid chain 7.5 Å from the bilayer centre. The distance between 9-AS and DOX molecule is 24.8 Å as determined by a FRET assay.

Confocal microscopy on fixed cells indicate that A431 and A549 cell lines use the endosomal pathway for DOX@DODAB:MO(1:2) liposome uptake. A temporally phased uptake was observed when compared with commercially available liposomal solution Doxil® and free DOX. A431 cells uptake DOX faster than A549, live cell experiments

of A431 cells confirmed that DODAB:MO(1:2) liposomal system releases the DOX in controlled way.

The location of the DOX towards the interior of the liposome could have interesting applications for drug delivery, and may be able to deliver more DOX at once without dimerization occurring.

8. OUTLOOK

In the future, testing the DODAB:MO(1:2) liposomal system through more comprehensive *in vivo* and 3D *in vitro* systems will allow the treatment system to be further developed, hopefully resulting in a new and better drug delivery systems on the market to help cancer patients.

To develop a deeper understanding of the internalization and release mechanism relevant, tissues shall be studied and thereby shall help to better identify the most suited nanocarrier candidates to advance towards the later stage of clinical trials.

To advance efficiently the design process of novel nanotherapeutics, in future work I propose to use and develop a combination of spectroscopy and imaging techniques to follow the nanocarrier internalization and drug release. Identification of the differences in nanocarrier - cell interaction, e.g. when comparing cancer/non-cancer cells, drug resistant/non-resistant cells and/or when comparing the effect of different commercially available and/or innovative potentially optimized nanoformulations with classical direct drug delivery shall be performed.

By using *in vitro* cell assays, relevant basic interaction mechanisms between cells and nano drug carriers can be answered. Additionally, to reach more realistic prognosis of nanotherapy efficacy and targeted delivery in the human body, more realistic human tissue models based on the combination of various cancerous and non-cancerous *in vitro* engineered models and deep tissue imaging techniques are required to assess drug internalization, delivery and drug release. Ideally, biomimetic tissue model should simulate *in vivo* conditions to observe relevant release mechanisms.

9. REFERENCES

Almeida, F.H., 2009. *Encapsulation of Bovine Serum Albumin (BSA) in DODAB:MO (1:2) Liposomes for Enhanced Antigen Immunization*. University of Minho.

American Cancer Society, 2015. Types of chemotherapy drugs. Available at: http://www.cancer.org/treatment/treatmentsandsideeffects/treatmenttypes/chemotherapy/chemotherapyprinciplesanin-depthdiscussionofthetechniquesanditsroleintreatment/chemotherapy-principles-types-of-chemo-drugs [Accessed January 1, 2015].

ATCC, 2014. A-431.

Bao, A. et al., 2004. Direct 99m Tc Labeling of Pegylated Liposomal Doxorubicin (Doxil) for Pharmacokinetic and Non-Invasive Imaging Studies. *Pharmacology*, 308(2), pp.419–425.

Barenholz, Y., 2012. Doxil - The first FDA-approved nano-drug: Lessons learned. *Journal of Controlled Release*, 160(2), pp.117–134. Available at: http://dx.doi.org/10.1016/j.jconrel.2012.03.020.

Berberan-Santos, M.N. & Prieto, M.J.E., 1987. Energy Transfer in Spherical Geometry. *Chem. Soc.*, 83(8), pp.1391–1409.

Berg, H.C., 1993. *Random Walks in Biology*, Princeton, NJ: Princeton University Press.

Dailey, M.E., 2016. Education in Microscopy and Digital Imaging. Live-cell imaging techniques. Available at: http://zeiss-campus.magnet.fsu.edu/articles/livecellimaging/techniques.html [Accessed April 20, 2016].

Van Dijck, A., 2013. *Bovine Serum Albumin (BSA) Encapsulated in DODAB:MO (1:2) Liposomes for Targeted Drug Delivery: Development and Characterization*. GHENT UNIVERSITY.

Drugbank.ca, 2013. Doxorubicin. Available at: http://www.drugbank.ca/drugs/DB00997 [Accessed April 4, 2016].

Ducat, E. et al., 2011. Cellular uptake of liposomes monitored by confocal microscopy and flow cytometry. *Journal of Drug Delivery Science and Technology*, 21(6), pp.469–477. Available at: http://dx.doi.org/10.1016/S1773-2247(11)50076-0.

Eisinger, J. & Flores, J., 1982. CYTOSOL-MEMBRANE INTERFACE OF HUMAN ERYTHROCYTES A Resonance Energy Transfer Study. *Biophysics*, 41, pp.367–379.

Elron-Gross, I., Glucksam, Y. & Margalit, R., 2009. Liposomal dexamethasone-diclofenac combinations for local osteoarthritis treatment. *International Journal of Pharmaceutics*, 376(1-2), pp.84–91.

Fujimoto, J. & Brezinsky, M., 2003. *Biomedical Photonics HANDBOOK*,

Gavin, H., 2015. The Levenberg-Marquardt method for nonlinear least squares curve-fitting problems. *Department of Civil and Environmental Engineering Duke University*. Available at: Retrieved from http://people.duke.edu/~hpgavin/ce281/lm.pdf [Accessed January 5, 2016].

Haldar, S. et al., 2012. Depth-dependent heterogeneity in membranes by fluorescence lifetime distribution analysis. *Journal of Physical Chemistry Letters*, 3(18), pp.2676–2681.

Immordino, L., Dosio, F. & Cattel, L., 2006. Stealth liposomes: review of the basic science, rationale, and clinical applications,. *International journal of nanomedicine*, 1(3), pp.297–315.

ISS inc., 2012. *ChronosBH Lifetime Spectrometer User Manual*, Champaign, Illinois.

ISS inc., 2015. Software Vinci. Available at: http://www.iss.com/fluorescence/software/vinci.html [Accessed January 4, 2016].

Kamps, J. & Scherphof, G.L., 2003. Liposomes in biological systems. In V. P. Torchilin & V. Weissig, eds. *Liposomes, A Practical Approach, 2nd ed.* New York: Oxford University Press, pp. 267–288.

Kwok, T.T. & Sutherland, R.M., 1991. EPIDERMAL GROWTH FACTOR REDUCES RESISTANCE TO DOXORUBICIN. , 76, pp.73–76.

Lakowicz, J.R., 2006a. *Instrumentation for Fluorescence Spectroscopy 2.1.*,

Lakowicz, J.R., 2006b. Quenching of Fluorescence. In *Principles of Fluorescence Spectroscopy*. pp. 277–330.

Laouini, A. et al., 2012. Preparation, Characterization and Applications of Liposomes: State of the Art. *Journal of Colloid Science and Biotechnology*, 1(2), pp.147–168. Available at: http://openurl.ingenta.com/content/xref?genre=article&issn=2164-9634&volume=1&issue=2&spage=147.

Lian, T. & Ho, R.J., 2001. Trends and developments in liposome drug delivery systems. *Journal of pharmaceutical sciences*, 90(6), pp.667–680.

Liu, X. & Huang, G., 2013. Formation strategies, mechanism of intracellular delivery and potential clinical applications of pH-sensitive liposomes. *Asian Journal of Pharmaceutical Sciences*, 8(6), pp.319–328. Available at: http://dx.doi.org/10.1016/j.ajps.2013.11.002.

Madeira, C. et al., 2011. Fluorescence methods for lipoplex characterization. *Biochimica et Biophysica Acta - Biomembranes*, 1808(11), pp.2694–2705. Available at: http://dx.doi.org/10.1016/j.bbamem.2011.07.020.

Malvern Instruments, 2000. Dynamic Light Scattering: An Introduction in 30 Minutes. , pp.1–8. Available at: Http://www.malvern.com/En/Products/Technology/Dynamic-Light-Scattering/ [Accessed March 29, 2016].

Malvern Instruments, 2013. *Zetasizer Manual* 1.1 ed., Worcestershire.

Mason, R.P., Rhodes, D.G. & Herbette, L.G., 1991. Reevaluating equilibrium and kinetic binding parameters for lipophilic drugs based on a structural model for drug interactions with biological membranes. *Journal of Medicinal Chemistry*, 34(3), pp.869–877. Available at: http://pubs.acs.org/doi/abs/10.1021/jm00107a001\nhttp://pubs.acs.org/doi/pdf/10.1021/jm00107a001.

Momparler, R.L. et al., 1976. Effect of adriamycin on DNA, RNA, and protein synthesis in cell-free systems and intact cells. *Cancer research*, 36(8), pp.2891–2895.

Nakanishi, T. et al., 2001. Development of the polymer micelle carrier system for doxorubicin. *Journal of Controlled Release*, 74(1-3), pp.295–302.

Neves Silva, J.P. et al., 2014. Tunable pDNA/DODAB:MO lipoplexes: The effect of incubation temperature on pDNA/DODAB:MO lipoplexes structure and transfection efficiency. *Colloids and Surfaces B: Biointerfaces*, 121, pp.371–379.

Oliveira, A.. . N., 2016. *Development of Monoolein-based lipofection vectors for therapeutic siRNA delivery*. University of Minho.

Oliveira, A.C.N. et al., 2015. Stealth monoolein-based nanocarriers for delivery of siRNA to cancer cells. *Acta Biomaterialia*, 25, pp.216–229. Available at: http://dx.doi.org/10.1016/j.actbio.2015.07.032.

Oliveira, I.M.S.C. et al., 2012. Aggregation behavior of aqueous dioctadecyldimethylammonium bromide/monoolein mixtures: A multitechnique investigation on the influence of composition and temperature. *Journal of Colloid and Interface Science*, 374(1), pp.206–217. Available at: http://dx.doi.org/10.1016/j.jcis.2012.01.053.

da Rocha, M.E.B., 2014. *Desenvolvimento de uma formulação lipossomal para entrega de um fármaco anticancerígeno*. Universidade do Minho.

Shukla, S., 2016. A REVIEW ARTICLE ON NANOPARTICLE. *PharmaTutor Edu Labs*, p.5. Available at: http://www.pharmatutor.org/articles/review-article-nanoparticle?page=0,0 [Accessed April 4, 2016].

Silva, J. et al., 2012. Development of dioctadecyldimethylammonium bromide/monoolein liposomes for gene delivery. In *Cell Interaction*. pp. 245–272. Available at: http://repositorium.sdum.uminho.pt/handle/1822/20399.

Silva, J. et al., 2011. DODAB:monoolein-based lipoplexes as non-viral vectors for transfection of mammalian cells. *Biochimica et Biophysica Acta - Biomembranes*, 1808(10), pp.2440–2449. Available at:

http://dx.doi.org/10.1016/j.bbamem.2011.07.002.

Silva, J.P.N. et al., 2014. Tunable pDNA/DODAB:MO lipoplexes: the effect of incubation temperature on pDNA/DODAB:MO lipoplexes structure and transfection efficiency. *Colloids and Surfaces B: Biointerfaces*, 121, pp.371–9. Available at: http://www.ncbi.nlm.nih.gov/pubmed/25023903.

Silva, J.P.N., Coutinho, P.J.G. & Oliveira, M.E.C.D.R., 2008. Characterization of monoolein-based lipoplexes using fluorescence spectroscopy. *Journal of Fluorescence*.

Thorn, C. et al., 2012. Doxorubicin pathways:pharmacodynamics and adverse effects. *Pharmacogenet Genomics*, 21(7), pp.440–446.

Thulborn, K.R. et al., 1979. The use of n-(9-anthroyloxy) fatty acids to determine fluidity and polarity gradients in phospholipid bilayers. *BBA - Biomembranes*, 558(2), pp.166–178.

Tian, Y. et al., 2003. Titration Microcalorimetry Study : Interaction of Drug and Ionic Microgel System.

Wahl, M., 2014a. Time-correlated single photon counting. *Technical Note*, pp.1–14. Available at: http://www.picoquant.com/images/uploads/page/files/7253/technote_tcspc.pdf.

Wahl, M., 2014b. Time-Correlated Single Photon Counting The Principle of Time-Correlated. , pp.1–14.

Wikimedia, 2007a. Chemical Structure of Triton X-100. Available at: https://en.wikipedia.org/wiki/Triton_X-100#/media/File:Triton_X-100.png [Accessed April 21, 2016].

Wikimedia, 2016. Hemoglobin. Available at: https://commons.wikimedia.org/wiki/File:Heme_b.svg [Accessed April 21, 2016].

Wikimedia, 2007b. Skeletal formula of dipalmitoylphosphatidylcholine (DPPC). Available at: By Fvasconcellos - Own work, Public Domain, https://commons.wikimedia.org/w/index.php?curid=1738613 [Accessed April 21, 2016].

Wikimedia, 2008. Sodium dodecyl sulfate. Available at: https://commons.wikimedia.org/wiki/File:Sodium_dodecyl_sulfate.svg [Accessed April 21, 2016].

World Health Organization, 2015. Cancer. Fact sheet N°297. Available at: http://www.who.int/mediacentre/factsheets/fs297/en/ [Accessed December 23, 2015].

APPENDIX A: MATLAB FITTING ALGORITHM

Program 1. *Matlab fitting algorithm*

```
%% Run fit_lsq

clear x xdata ydata tau

load('matlab.mat')    %structure containing data for all samples
intensity1=str2double(tcspc(1, 8).Dataset(:,4,1)); %finding intensity values
t_start=9.9;        %time interval start
t_end=34;           %time interval end

g=max(intensity1);
[s1,s2]=find(intensity1 == g); %finding at which time point max peak occurs
for time axis correction
xdata=x-x(s1,1);
i_start=interp1(x,1:length(x),t_start,'nearest');
i_end=interp1(x,1:length(x),t_end,'nearest');
xdata=xdata(i_start:i_end,1);
xdata=xdata';               %finding the exact time vector

tau=[1, 5, 0.1]; % Starting guess
intensity = smooth(intensity1,9);
ydata = intensity(i_start:i_end,1)./max(intensity);
ydata =ydata';

[F]= fit_lsq( xdata,ydata,tau )  %calling the least squares fitting function
F.fit=(F.b*exp(-(xdata)./F.tau1)+(1-F.b)*exp(-
(xdata)./F.tau2))*max(intensity);
F.chi=sum((F.fit-ydata).^2)./sum(ydata);
set(0,'defaultlinelinewidth',2)
figure;plot(xdata,F.fit,x-x(s1,1),intensity1)
legend('Fitted function','Measured data')
xlabel('t, ns', 'Fontsize', 14);
ylabel('Intensity', 'Rotation', 90, 'Fontsize', 14);
set(gca, 'XLim',[0,100])
```

Program 2. *Matlab fitting function*

```
function F = fit_lsq( xdata,ydata,tau )
%fit_lsq function finds coefficients with best fit (with 0<b<1)
%   xdata - time vector
%   ydata - intensity vector
%   tau - initial guess
%   b - weighting factor of tau1 and tau2 (0<b<1)

function [y_fit]= get_fitcurve_2c(tau,xdata)
tau1=tau(1);
tau2=tau(2);
b=tau(3);
y_fit=(b*exp(-(xdata)./tau1)+(1-b)*exp(-(xdata)./tau2)); % equation that
has to be evaluated by lsqcurvefit

end
fhandle = @get_fitcurve_2c;
```

```
        options = optimoptions('lsqcurvefit','MaxFunEvals',50000, 'MaxIter',
                                                    50000);% optimization of options
    [tau,resnorm] = lsqcurvefit(@get_fitcurve_2c,tau,xdata,ydata,[0 0 0],[inf
                          inf 1],options) %starts at X0 and finds coefficients
                                                                  F.tau1=tau(1);
                                                                  F.tau2=tau(2);
                                                                     F.b=tau(3);

                                                                          end
```

APPENDIX B: TCSPC MEASUREMENTS

Table 1. *Lifetime values,ns*

	Matlab				ISS			
[DOX]	3AS_m	6AS_m	9AS_m	12AS_m	3AS_ISS	6AS_ISS	9AS_ISS	12AS_ISS
0	6.903524	6.141001	7.333535	8.742043	7.596398	7.002174	9.034092	10.69319
20	6.537212	5.874523	7.022964	8.609434	7.250448	6.958782	8.607769	10.58293
40	6.789805	5.626665	6.920607	8.535996	7.563962	6.818364	8.431787	10.37803
60	6.706415	5.745945	7.100697	8.517346	7.493347	6.783929	8.861613	10.614
80	6.650808	5.649955	6.862521	8.467972	7.291034	6.798383	8.548535	10.6307
100	6.481339	5.618484	6.718419	8.266475	7.32175	6.893652	8.542267	10.5186

Table 2. *χ^2 values*

	Matlab				ISS			
[DOX]	3AS_m	6AS_m	9AS_m	12AS_m	3AS_ISS	6AS_ISS	9AS_ISS	12AS_ISS
0	1.04	1.02	1.06	1.04	1.03	1.00	1.00	0.99
20	0.96	1.00	1.03	1.03	0.97	0.96	0.97	1.02
40	1.01	1.06	1.03	1.02	0.98	1.03	0.98	1.00
60	1.04	0.98	1.01	1.03	0.99	1.01	0.98	1.00
80	0.99	1.06	1.06	1.02	1.00	1.01	1.03	1.01
100	1.00	1.04	0.98	1.06	1.03	1.03	0.98	1.04

APPENDIX C: FLUORESCENCE EMISSION DATA SMOOTHING

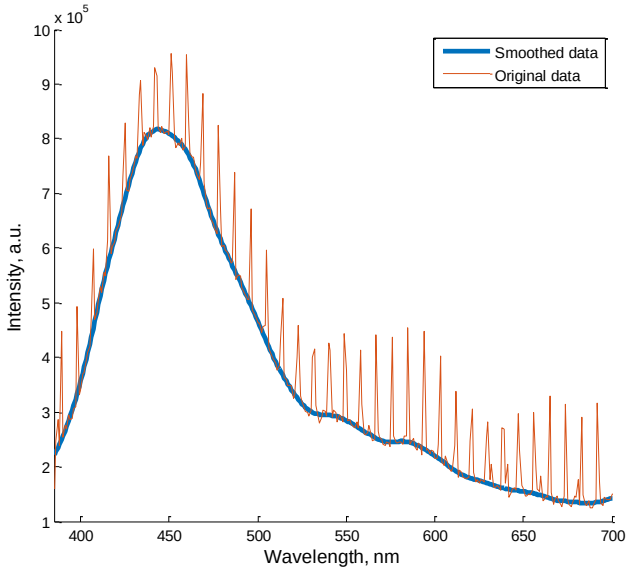

Figure 1. *Example of recorded original steady state fluorescence emission data forDODAB:MO liposomes labelled with 6 AS probe and containing 20 μM of DOX (orange) and fitted smoothed data curve (blue)*

Due to spectrometer's malfunction, in addition to the broad fluorescence spectrum narrow equidistant artefacts form part of the recorded spectra (Figure 1). The data curve was processed using Matlab function that smooths the response data ('rloess'). It assigns lower weight to outliers in the regression. Local regression using weighted linear least squares and a 2^{nd} degree polynomial model was used. Smoothed data sets were then background corrected by subtracting the minimum value from each measurement.

APPENDIX D: ABSORBANCE VALUES

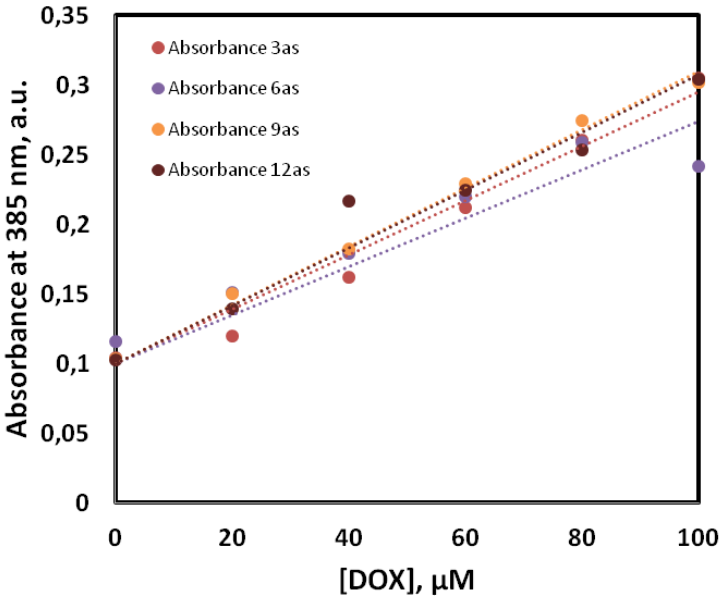

Figure 2. *Absorbance values of the n-AS probes inserted in DODAB:MO liposomes determined at 385 nm as a function of DOX concentration.*

APPENDIX D: CELL UPTAKE STUDIES

Program 3. *Fiji macro for increased brightness/contrast settings*

```
dir1 = getDirectory("Choose Source Directory ");
dir2 = getDirectory("Choose Destination Directory ");
list = getFileList(dir1);
setBatchMode(true);
for (i=0; i<list.length; i++)
{showProgress(i+1, list.length);
 open(dir1+list[i]);
run("Split Channels");
close();
run("Z Project...", "projection=[Sum Slices]");
run("Gaussian Blur...", "sigma=0.30 scaled");
run("8-bit");

AUTO_THRESHOLD = 5000;
 getRawStatistics(pixcount);
 limit = pixcount/10;
 threshold = pixcount/AUTO_THRESHOLD;
 nBins = 256;
 getHistogram(values, histA, nBins);
 k = -1;
 found = false;
 do {
         counts = histA[++k];
         if (counts > limit) counts = 0;
         found = counts > threshold;
 }while ((!found) && (k < histA.length-1))
 hmin = values[k];

 k = histA.length;
 do {
         counts = histA[--k];
         if (counts > limit) counts = 0;
         found = counts > threshold;
 } while ((!found) && (k > 0))
 hmax = values[k];

 setMinAndMax(hmin, hmax);
run("yellowtored");
run("Invert LUT");
run("Calibration Bar...", "location=[Upper Left] fill=White label=Black num-
ber=3 decimal=0 font=12 zoom=1 overlay");
run("Scale Bar...", "width=100 height=4 font=14 color=Black background=None
location=[Lower Right] bold");
saveAs("PNG", dir2+list[i]);
 close();
}
```

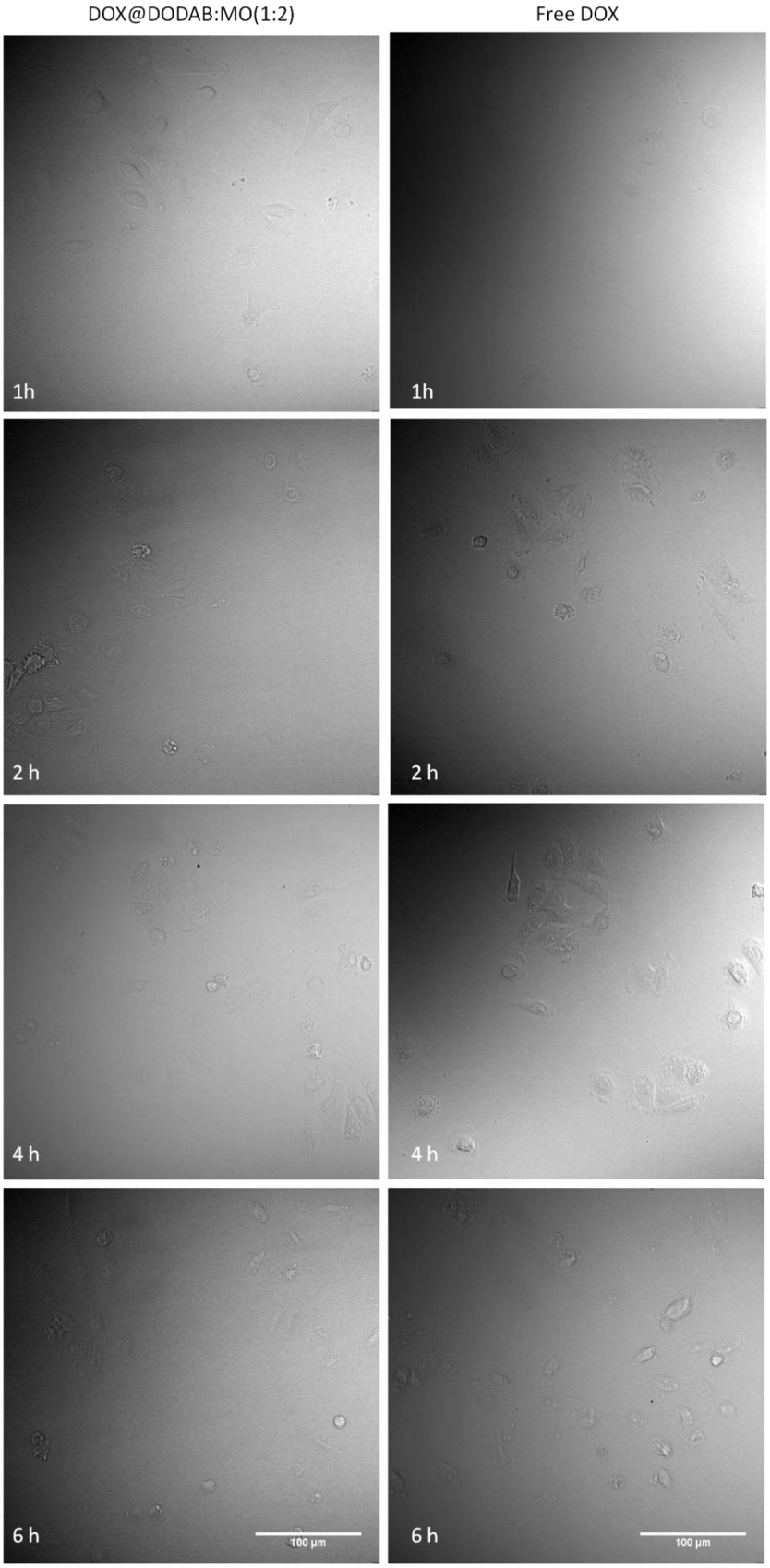

Figure 3. *Transmission images of A549 cells incubated with DOX@DODAB:MO and free DOX*

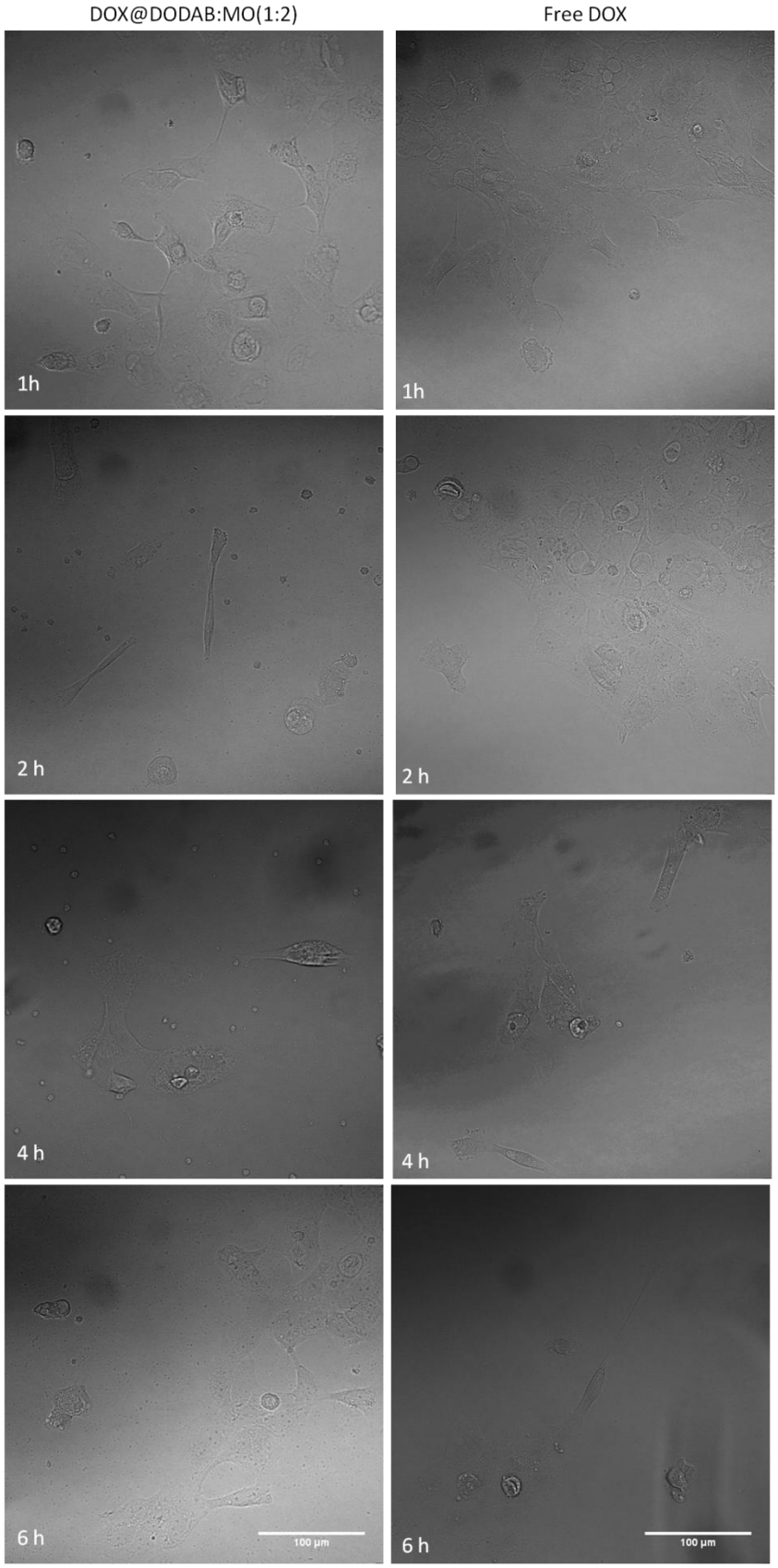

Figure 4. *Transmission images of A431 cells incubated with DOX@DODAB:MO and free DOX*

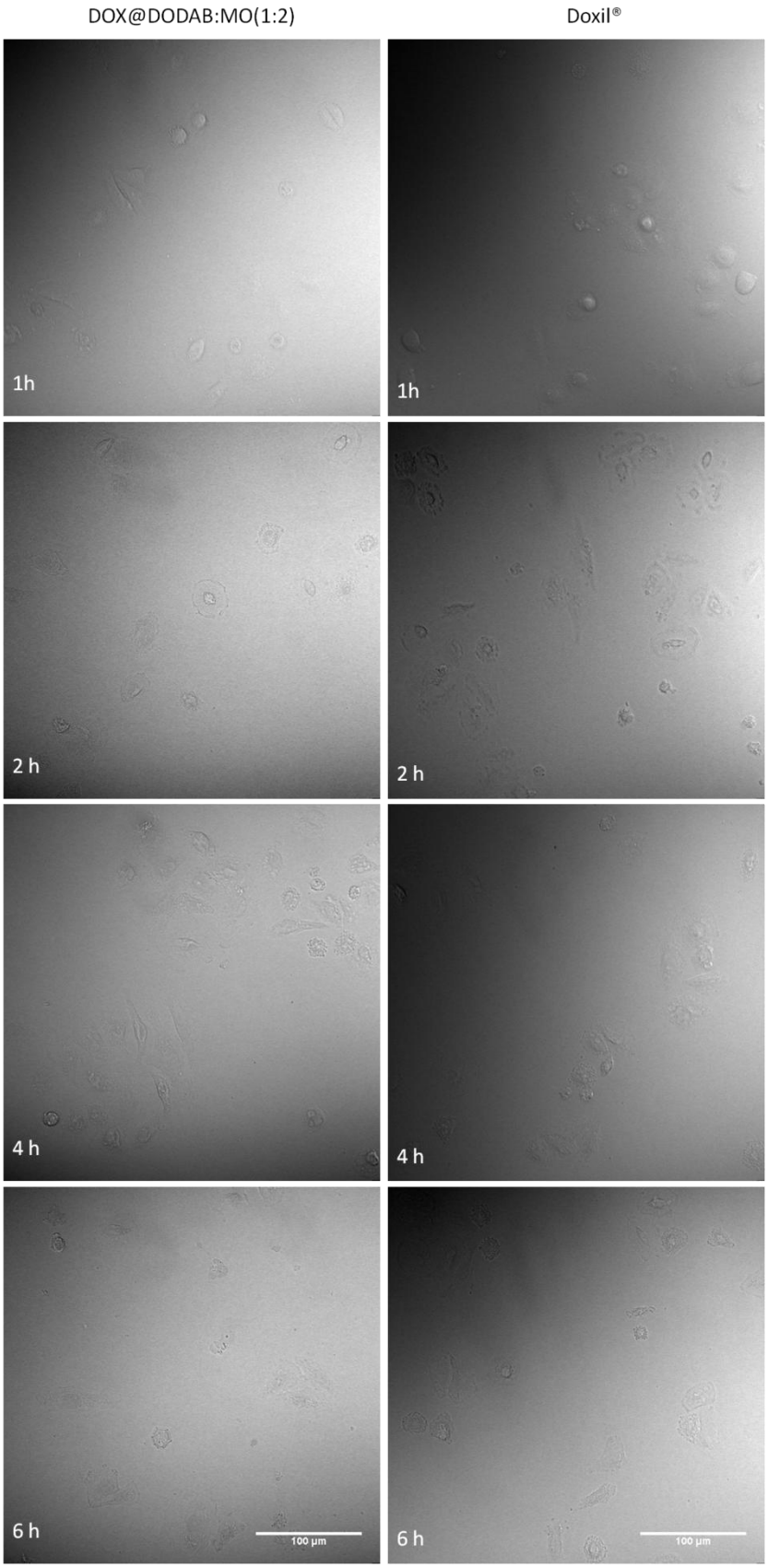

Figure 5. *Transmission images of A549 cells incubated with DOX@DODAB:MO and Doxil®*

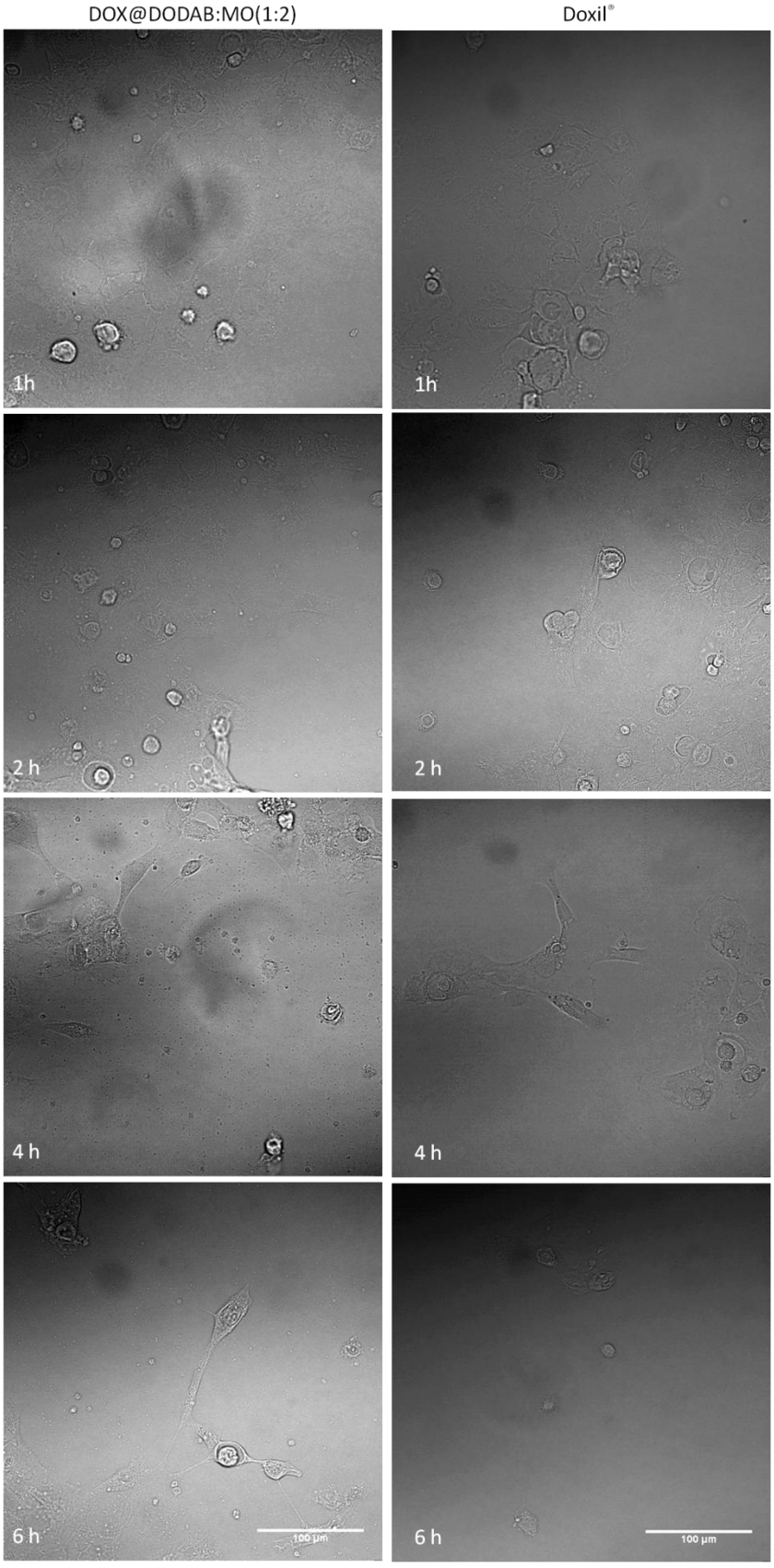

Figure 6. *Transmission images of A431 cells incubated with DOX@DODAB:MO and Doxil®*